Title: Atlas of innate immune responses to experimental cholera and IL22 treatment demonstrates protection by mucus-secreting cells

Authors: Masataka Suzuki[1], Yuko Hasegawa[1]†, Hailong Zhang[1]‡, Zhu Liang[1], Guodong Tie[2], Ramesh A. Shivdasani[2], Matthew K. Waldor[1]*

Affiliations:

1. Department of Microbiology, Harvard Medical School, Division of Infectious Diseases, Brigham & Women's Hospital, Howard Hughes Medical Institute, Boston, MA 02115.
2. Department of Medical Oncology and Center for Functional Cancer Epigenetics, Dana-Farber Cancer Institute, Boston, MA 02215, USA; Department of Medicine, Harvard Medical School, Boston, MA 02115, USA; Harvard Stem Cell Institute, Cambridge, MA 02138, USA.

†. Current affiliation: Molecular Biology and Genetics, Cornell University, Ithaca, NY, 14853.

‡. Current affiliation: Medical University of South Carolina, Charleston, SC 29425.

* Corresponding author. Email: mwaldor@research.bwh.harvard.edu

Abstract: The diarrheal disease cholera remains a global threat. However, knowledge of the innate immune defenses in the small intestine that protect against the causative agent, *Vibrio cholerae,* is limited. Here, single-cell RNA-sequencing of epithelial and immune cells mapped gene expression patterns in the infant mouse small intestine and revealed changes in response to *V. cholerae* infection and treatment with an IL22 Fc-fusion protein. Infection increased the abundance of an enterocyte subtype that highly expressed defense-associated functions and stimulated production of IL22, a cytokine linked to epithelial integrity, from group 3 innate lymphoid cells. Administration of IL22Fc increased production of vibriocidal Reg3β from enterocytes and the abundance of secretory lineage and Muc2-producing goblet cells, which secreted mucus into the intestinal crypts, impairing *V. cholerae* association with the epithelium. These IL22-mediated responses limited *V. cholerae* intestinal colonization and protected mice from diarrhea and death. These observations suggest enterocyte specialization in mucosal defense, identify mechanisms of IL22-mediated protection, and point to host-directed approaches for cholera therapeutics.

Main Text:

Introduction

Vibrio cholerae, the cholera pathogen, infects several million people and causes tens of thousands of deaths annually, particularly in low- and middle-income countries in south Asia and Africa[1]. Cholera patients can lose many liters of diarrheal fluid within hours and die from dehydration without proper treatment[2]. *V. cholerae* is a curved, highly motile Gram-negative rod that associates with the epithelium of the human small intestine (SI), the site of colonization. Various *V. cholerae* genes and processes, including its Tcp pilus along with flagellar-based motility are important for intestinal colonization[3]. While replicating along the epithelium, the pathogen secretes cholera toxin, whose activities largely account for the secretory diarrhea characteristic of cholera.

Knowledge of adaptive immune responses to natural and experimental *V. cholerae* infection in humans has expanded in recent years[4]. Infection leads to the generation of protective antibody responses that can limit intestinal colonization and diarrhea[5]. However, despite more than a century of studies of cholera pathogenesis[6–8], the comprehensive understanding of epithelial and innate immune responses to *V. cholerae* infection in the small intestine is fairly limited, though human biopsy studies have suggested roles for neutrophil infiltration, and elevated abundance of inflammation-associated and antimicrobial proteins including TNF, IL1β, IL23, lactoferrin, LPLUNC1 and defensin[6–11]. Epithelial cells represent a critical barrier preventing pathogens or commensal bacteria from entering host tissues, and these cells produce physical (e.g., mucus) and chemical (e.g., reactive oxygen species, antimicrobial peptides) obstacles that impede microbial invasion of deeper tissues[6]; epithelial cells also initiate immune responses when the epithelial barrier is compromised[12]. In cholera naïve individuals, such innate responses are likely to be critical determinants of survival given that severe cholera can kill infected individuals within a day of infection, before adaptive immune responses are generated[2].

Modeling human pathogenesis, *V. cholerae* robustly colonizes the small intestine (SI) of infant mice without antibiotic pre-treatment. Furthermore, colonization of the infant mouse SI depends on the Tcp pathogenicity island, as is the case in humans[13]. Here, we characterized intestinal epithelial and immune cell responses to *V. cholerae* infection in infant mice using single-cell RNA sequencing (scRNA-seq). Our findings uncover patterns of mucosal innate defense and reveal that IL22 therapy shifts stem cell differentiation of intestinal stem cell daughters toward the secretory lineage, which protects against infection by impairing pathogen association with the epithelium. These findings could point to new approaches for cholera treatment.

Results

V. cholerae infection triggers antimicrobial responses in intestinal epithelial cells

scRNA-seq analysis of epithelial cells harvested from the SI of postnatal day 5 (P5) infant mice revealed 15 cell clusters, including various enterocyte subtypes, goblet cells, and enteroendocrine cells (Fig. 1ab, Extended Data Fig. 1ab, Supplementary Table 1). The expression profiles in the 11 enterocyte clusters and stem cells likely distinguish where they are located along the crypt-villus axis[13] (Extended Data Fig. 1c). However, Paneth and tuft cells

were not detected (Extended Data Fig. 1d), revealing the developmental immaturity of the epithelial defense system in P5 mice[14].

V. cholerae infection altered the transcriptional profiles in nearly all clusters of SI epithelial cells, particularly in the distal SI, where the pathogen burden is 10-100x greater than in the proximal SI[15] (Extended Data Fig. 2a, Supplementary Table 2, 3). Pathway analyses showed prominent upregulation of inflammatory signaling and hypoxia pathways across almost all epithelial cell clusters (Fig. 1cd, Extended Data Fig. 2b). There were also cell type-specific infection-induced perturbations, such as in metabolic pathways (Fig. 1d, Extended Data Fig. 2c), suggesting that infection stimulates distinct regulatory networks across epithelial cell types; for example, stem cells exhibited prominent increases in expression of genes linked to the MYC pathway, suggesting that infection triggers stem cell proliferation (Extended Data Fig. 2d). Highly induced genes in stem cells were generally different than those in most enterocyte populations and goblet cells (Fig. 1c, Extended Data Fig. 2e).

There were minimal differences in the relative abundances of epithelial clusters in the proximal SI in control vs infected animals (Extended Data Fig. 1b, 2f). In contrast, there was a marked increase in the abundance (12.6-fold) of cluster 5 enterocytes in the distal SI of infected animals (Fig. 1b, e). Cluster 5 enterocytes expressed the Reg3β and Reg3γ antimicrobial peptide genes even in the absence of infection (Extended Data Fig 3a), suggesting that this epithelial subset is specialized for defense against infection. With infection, cluster 5 enterocyte highly expressed genes classed as defense responses, including *Il18*, as well as genes encoding fibrinogen proteins, *Fga* and *Fgb*, which are traditionally associated with clotting[16] (Fig. 1f, Extended Data Fig 3a). In contrast, infection was associated with reduced expression of several metabolic pathways in this enterocyte subset (Extended Data Fig. 2c). Single molecule RNA FISH using probes for cluster 5 marker genes confirmed that these cells were found in the epithelium and that their abundance increased with infection; cluster 5 enterocytes were primarily located toward the base of the villus (Fig 1g and Extended Data Fig 3b), the site where *V. cholerae* primarily localizes as well[15].

We conducted lineage tracing to investigate whether the infection-associated increase in abundance of cluster 5 enterocytes arose from Lgr5+ stem cells during the 20-hour infection period or from enterocytes already present on villi. $Lgr5^{Cre(ER-T2)}$/ $Rosa26R^{LSL-TdTomato}$ animals, which express a Lgr5-dependent tamoxifen-inducible tdTomato, were infected with *V. cholerae*. After 20 hours of infection, only 0.2 % of cluster 5 (*Sult6b2*+) cells were tdTomato+ (Fig. 1h-j). To test whether cluster 5 cells were derived from transient amplifying cells or had themselves expanded, we administered the S-phase reagent EdU at the time of infection or 2 hours before tissue harvest. When tissues were examined, only 5.2 % or 0.8 % of cluster 5 (*Sult6b2*+) cells were EdU+ when this reagent was administered at the time of infection or 2 hours prior to tissue sampling respectively (Extended Data Fig. 3c-e). Together these findings indicate that the infection-associated expansion of cluster 5 enterocytes originates from another enterocyte population and did not differentiate from stem cells, or self-amplify in response to the infection. Moreover, RNA velocity analysis of our scRNA-seq data corroborated this idea, predicting that cluster 5 cells originated from $Lgr5^{-}$negative, MKi67-negative cells (Extended Data Fig. 3f), and buttressing the conclusion that the majority of cluster 5 cells originate from another subset of enterocytes.

Infection stimulated increased expression of *Reg3b* and *Reg3g* in all the epithelial cell clusters in the distal SI (Extended Data Fig 3a). Immunostaining established that Reg3β is highly expressed in epithelial cells towards the upper crypt and middle section of villi in infected

127 animals (Fig. 1k, Extended Data Fig 3g). Moreover, Reg3β staining was often colocalized with
128 *V. cholerae* microcolonies found on the epithelial surface (Fig.1k-m, Extended Data Fig 3g),
129 suggesting that this lectin is secreted and bound to the pathogen during infection. Together, these
130 analyses reveal that *V. cholerae* infection can shifts the functions of enterocytes towards defense
131 both by reprogramming gene expression in many enterocyte populations and by increasing the
132 abundance of a distinct, defense-associated subset (cluster 5).
133
134 ***V. cholerae* infection stimulates IL22 expression in type 3 innate lymphoid cells**
135 Crosstalk between epithelial and immune cells found in the SI lamina propria plays a key
136 role in host protection against enteric bacterial infection[12,17]. We also carried out scRNA-seq
137 analysis of CD45+ immune cells isolated from the SI lamina propria of control and *V. cholerae*-
138 infected P5 infant mice. Cell cluster analysis based on marker gene expression revealed 32
139 clusters in both the proximal and distal SI (Fig. 2a, Extended Data Fig. 4a-c, Supplementary
140 Table 1). The cell types previously observed in adult animals[18] were also detectable in the SI of
141 P5 neonates with the exception of plasma cells (Extended Data Fig. 4d). As observed for
142 epithelial cell responses, there were more differentially expressed genes in the CD45+ cells
143 isolated from the distal vs. proximal SI and considerable variability in infection-induced changes
144 in gene expression among cell clusters (Fig. 2b, Extended Data Fig. 5a, Supplementary Table 4,
145 5). Pathway analysis revealed that, in contrast to scRNA-seq studies in *V. cholerae*-infected
146 zebra fish, where the pathogen reduced interferon signaling in the intestine[19], interferon response
147 pathway genes were prominently induced in B and T cells, which express the receptors for Type
148 I (α and β) and II (γ) interferon, *Ifnar1/Ifnar2* and *Ifngr1/Ifngr2* respectively, while innate
149 lymphoid cells responded to pro-inflammatory IL17, IL23 signaling but not to interferons (Fig.
150 2b-d, Extended Data Fig. 5bc). NK cells may be the source of interferon gamma (Extended Data
151 Fig. 5c), but producer(s) of Type I and III (λ) interferon were not apparent.
152 Differential expressed gene (DEG) analyses uncovered that gene expression patterns in
153 Type 3 LTi-like innate lymphoid cell (LTi-like ILC3) are prominently altered by infection (Fig.
154 2b). Cell-cell communication inference[20] was used to identify potential signaling between lamina
155 propria LTi-like ILC3 and epithelial cells. Several pathways were inferred, including IL22-
156 IL22ra1/IL10rb signaling from LTi-like ILC3 to epithelial cells (Fig. 2e). We focused additional
157 analyses on IL22 signaling because this cytokine was highly up-regulated by *V. cholerae*
158 infection (> 16-fold increase, adjusted p-value 3.24×10^{-38}) (Supplementary Table. 5) and is
159 known to promote epithelial barrier integrity[21–25]. Flow cytometry analysis and whole mount
160 staining corroborated the increased number of IL22+ cells, which were primarily ILCs and not
161 γδT cells and found in the lamina propria and among intraepithelial lymphocytes (IEL) (Fig. 2fg,
162 Extended Data Fig. 5d). Quantitative PCR analysis with IL22 knockout animals confirmed that
163 *V. cholerae* infection-induced expression of *Reg3b* and *Reg3g* depends on IL22 signaling
164 (Extended Data Fig. 5e), as observed in studies with other enteric pathogens [22,26]. Furthermore,
165 cluster 5 enterocyte marker genes induced by *V. cholerae* infection (Fig. 1g, Extended Data Fig.
166 3a) were not induced in IL22 knockout mice (Fig. 2h), suggesting that IL22 signaling promotes
167 the generation of this defense-associated enterocyte subset.
168 Thus, similar to epithelial cell responses, transcriptional responses to *V. cholerae*
169 infection in lamina propria immune cells were cell type-specific and more pronounced in the
170 distal SI. Also, among lamina propria innate immune cells, increased ILC3 expression of
171 regulatory cytokines, including IL22, was notable.
172

173 **Il22 protects infant mice from *V. cholerae* intestinal colonization and diarrhea**
174 Since IL22 has been linked to intestinal defense[21–25] and transcriptional profiling
175 suggested that *V. cholerae* infection stimulates an IL22-based signaling axis between lamina
176 propria ILC3 cells and the epithelium, we investigated whether this cytokine could impact the
177 course of *V. cholerae* infection in suckling mice. Because of the low expression of IL22 in very
178 young animals[27], we speculated that the administration of exogenous IL22 could change the
179 outcome of *V. cholerae* infection in P5 animals. Infant animals were given two doses of an
180 IL22Fc protein[28] at 24 and 0 hours before challenge with *V. cholerae* (Fig. 3a). This prophylactic
181 regimen of IL22Fc administration markedly decreased the *V. cholerae* burden in both the
182 proximal and distal SI (Fig 3b, Extended Data Fig. 6ab). In contrast, administration of
183 recombinant Il17a or Il17f, which were also activated in LTi-ILC3 by *V. cholerae* infection, or
184 Ifnβ or Ifnγ, whose receptor downstream signaling was activated in T, B and myeloid cells (Fig.
185 2cd, Extended Data Fig. 5b), did not influence *V. cholerae* colonization (Extended Data Fig. 6a-
186 d).
187 A bacterial-barcoding strategy was used to determine whether IL22-treatment strengthens
188 the initial bottleneck that limits *V. cholerae* colonization and/or prevents subsequent replication.
189 Amplicon sequencing and the STAMPR analytic pipeline monitor the diversity of otherwise
190 isogenic barcoded bacteria to quantify the number of cells that survive colonization bottlenecks
191 to initiate infection, referred to as the 'founding population'[29]. STAMPR revealed that both the
192 founding population (Ns) and net replication (CFU/Ns) in the distal SI were reduced in treated
193 animals (Fig. 3cd). These results suggest that IL22Fc both limits net replication and tightens the
194 host bottleneck, restricting the number of niches in the distal SI that are permissive for *V.*
195 *cholerae* replication or killing cells before they become founders.
196 When *V. cholerae*-infected animals are left with a dam and monitored for survival, they
197 develop diarrhea, lose weight, and generally die within 60 hours (Fig. 3e-g). In marked contrast,
198 in animals treated with IL22Fc, no weight loss, diarrhea, or death was observed (Fig. 3e-g). In
199 fact, the treated mice gained weight and at 60 hours had either entirely cleared *V. cholerae* or had
200 dramatically lower pathogen burdens than observed in the moribund control animals (Fig. 3h).
201 Only a single dose of IL22Fc 24 or 48 hours before infection was sufficient to impair *V. cholerae*
202 colonization (Extended Data Fig. 6ab), while IL22Fc treatment 5 days prior to infection had
203 limited effect (Extended Data Fig. 6e). Administration of IL22Fc 5 hours post *V. cholerae*
204 infection was sufficient to sustain the body weight of infant mice and prolong their survival,
205 suggesting that this treatment could be beneficial even after infection (Extended Data Fig. 6fg).
206 Together, these findings suggest that IL22 may have clinical value in preventing or even treating
207 cholera.
208 We also tested whether prophylactic IL22Fc could reduce the colonization of other
209 enteric pathogens in infant mice. IL22Fc markedly limited *Citrobacter rodentium* colonization in
210 the SI and colon (Extended Data Fig.6h). However, IL22Fc administration only led to a modest
211 reduction in *Salmonella enterica* serovar Typhimurium intestinal colonization and did not reduce
212 the pathogen burden in the liver or spleen (Extended Data Fig.6i), suggesting that the treatment
213 did not influence pathogen dissemination. These results suggest that IL22Fc treatment is potent
214 at impairing the intestinal colonization of extracellular pathogens in infant animals.
215
216
217 **Elevated requirement for *V. cholerae* motility in IL22 treated animals**

To understand how IL22Fc-treatment alters the SI milieu, we compared *V. cholerae's* genetic requirements for intestinal colonization in IL22Fc-treated and control mice using a transposon insertion site sequencing (Tn-seq) screen (Fig. 4a). In this genome-scale bacterial loss of function screen, comparisons of the abundances of transposon insertions in genes in the inoculum (input) to plated intestinal homogenates (output) are used to infer the genetic requirements for growth *in vivo*; reductions in the abundance of insertions in a gene in the output sample relative to the input suggests the gene promotes growth in the intestine. As expected, transposon insertions in genes encoding essential colonization factors, such as genes required for the biogenesis of the toxin-coregulated pilus (Tcp), were similarly depleted (compared to the inoculum) in both IL22Fc-treated and vehicle (PBS)-treated animals (Fig. 4b and Supplementary Table 6). In contrast, insertions in genes depleted more in IL22Fc-treated vs control animals compared to the inoculum represent genes that are more important for intestinal colonization in the IL22Fc-treated host. Notably, the relative depletion of insertions in 22 genes related to motility were 4-32x greater in IL22Fc-treated vs control animals (Fig 4b,c and Extended Data Table. 1), suggesting that motility is more important for *V. cholerae* colonization in IL22Fc-treated animals. Non-motile strains with deletions in genes important for flagellar assembly (*fliI* and *flgD*) and flagellar-based motility (*motB*)[30] were created, and competition assays against wild-type strains corroborated the heightened importance of motility in IL22Fc-treated mice (Fig. 4d). We hypothesized that the increased importance of motility for colonization in the IL22Fc-treated mice reflects the role of motility in *in vivo* pathogen localization. Consistent with this idea, the fraction of luminal vs tissue-associated *V. cholerae* (Fig. 4e,f) was ~86x greater in the IL22Fc-treated mice, demonstrating that IL22Fc treatment alters the intestine in a manner that impedes the pathogen from reaching the epithelial surface. In fact, it was difficult to detect fluorescently tagged *V. cholerae* closely associated with the epithelium in the crypts of treated mice (Fig. 4g). Together, these observations suggest that at least in part, IL22Fc treatment restricts *V. cholerae* colonization by limiting the pathogen's access to the epithelial surface.

IL22 administration modifies the gene expression profiles and cellular composition of the SI epithelium

Treatment with IL22Fc significantly increased the length of the SI, but not the colon, without impacting the pups' body weight (Extended Data Fig. 7a-c), suggesting that this cytokine modifies the development of the SI. 36 hours after IL22Fc administration, scRNA-seq of the SI epithelium revealed a marked increase in the abundance of cluster 3 and 9 cells (Fig 5a,b, Supplementary Table 1). Moreover, IL22Fc treatment stimulated changes in the transcriptomes of all types of epithelial cells in the distal SI (Extended Data Fig. 7d). Unexpectedly, IL22Fc treatment reduced the expression of more genes than it increased in 13 of 14 clusters (Extended Data Fig. 7d, Supplementary Table 7). There was a trend toward reduced expression of genes linked to lipid and sugar metabolism pathways as well as cell cycle genes in enterocytes of IL22-treated mice (Extended Data Fig. 7e-g), consistent with previous studies that elucidated a role of IL22 signaling in metabolism[31]. For some genes, IL22Fc administration induced changes in all cell types (e.g. increased expression of antimicrobial peptides) and in other cell subsets gene expression changes were more specific. For example, this treatment only stimulated expression of pathways associated with cell cycle (Mitosis, E2F, and MYC Target) in stem cells (Extended Data Fig. 7e). We confirmed stem cell proliferation in IL22Fc-treated animals with EdU staining (Extended Data Fig. 7h-j), as reported[32]. Notably, in most enterocyte clusters, genes highly expressed in cluster 5 enterocytes from *V. cholerae* infected animals were

prominently upregulated by IL22Fc-treatment (Fig. 5c), suggesting that IL22 reprograms enterocytes to promote epithelial defense.

IL22 induces expression of vibriocidal *Reg3b*

Among upregulated genes, pathway analysis revealed that IL22Fc increased expression of genes linked to synthesis of antimicrobial peptides in all epithelial populations (Extended Data Fig. 8a). *Reg3b* and *Reg3g* were among the most highly induced genes by Il22Fc treatment (Extended Data Fig. 8a); IL22Fc-treatment markedly elevated expression of *Reg3b* and *Reg3g* 10,000-fold compared to untreated animals, and in treated mice there was no further increase in expression of these antimicrobial proteins (Extended Data Fig. 8b). The elevated expression of these antimicrobial proteins, which was also associated with IL22Fc treatment in a study of the colonic pathogen *Citrobacter rodentium* in adult mice[22], along with *Defa24*, likely explains why antimicrobial pathways were one of the enriched pathways associated with this treatment in all clusters (Extended Data Fig. 8ab). However, proteomic analysis of mucosal washes from control and IL22Fc-treated animals only identified abundant Reg3β in treated animals, whereas Reg3γ, Defa17 and Defa24 were not identified (Extended Data Fig. 8c). Immunohistochemical staining confirmed that Reg3β is expressed all along the crypt-villus axis in IL22Fc treated animals (Extended Data Fig. 8d). Reg3β has been reported to kill several species of both Gram-negative[33] and Gram-positive bacteria[34] *in vitro,* but susceptibility of *V. cholerae* to this lectin has not been reported. In laboratory culture, we found that recombinant Reg3β decreased *V. cholerae* survival in a dose-dependent fashion, whereas heat-inactivated Reg3β failed to kill *V. cholerae* (Fig. 5d). Furthermore, oral administration of recombinant Reg3β protein decreased the *V. cholerae* burden as well as the size of the founding population and pathogen proliferation particularly in the distal SI (Fig. 5e-g), further confirming the vibriocidal activity of Reg3β *in vivo*. P5 Reg3β$^{-/-}$ mice were as susceptible to *V. cholerae* intestinal colonization as heterozygous littermates (Fig. 5h). However, IL22Fc administration to Reg3β$^{-/-}$ animals did not reduce the *V. cholerae* burden, size of the founding population, or amount of net proliferation as potently as in Reg3β$^{+/-}$ littermates (Fig. 5h-j), suggesting that the increased expression of Reg3β in IL22Fc treated animals contributes to the protective effects of IL22 *in vivo*. Since Reg3β$^{-/-}$ animals were still protected from *V. cholerae* infection by IL22Fc treatment (Fig. 5h), other protective mechanisms beyond Reg3β induction likely exist.

IL22 treatment increases the abundance of secretory epithelial cells

IL22 signaling is thought to be important for Paneth cell maturation and maintenance[35,36]. In P5 animals, where Paneth cells are absent (Extended Data Fig. 1c), IL22Fc administration increased the proportion of cells in the secretory lineage (cluster 3, 9, 13), especially cluster 3 (Extended Data Fig. 9a). Cells in clusters 3 and 9 express *Atoh1* and *Spdef*, key transcription factors for secretory lineage differentiation into goblet, Paneth, enteroendocrine, or tuft cells[37]. Based on marker genes, including *Muc2* and absence of *Lyz1* (Fig. 6ab), cluster 3 resembles adult goblet rather than Paneth cells[38]. However, cluster 9 has lower expression of goblet cell markers and expressed stem cell markers *Lgr5* and *Olfm4* (Fig. 6ab), suggesting it represents secretory progenitors[39]. Cells expressing *Atoh1* and *Spdef* reside primarily in crypts (Fig. 6c-e), and histologic assessment confirmed increased abundance of Muc2+ mucus-containing (PAS+) cells in the crypts of IL22Fc treated mice (Fig. 6f-h). Atoh1$^{Cre(ER-T2)}$;Rosa26R$^{LSL-tdTomato}$ mice, which encode Atoh1-dependent tamoxifen-inducible tdTomato, confirmed that crypt-associated mucous cells express *Atoh1* or derive from Atoh1+ cells (Extended Data Fig. 9b-d). To ask

310 whether IL22Fc induces proliferation of secretory progenitor and goblet cells, we administered
311 EdU and IL22Fc at the same time (Extended Data Fig. 9e). Compared with control animals, the
312 numbers of EdU+ *Atoh1*+ cells were increased (Extended Data Fig. 9fg), indicating that IL22Fc
313 triggers proliferation of Atoh1+ secretory progenitors or goblet cells. Together, these findings
314 reveal that IL22Fc promotes secretory lineage and goblet cell development *in vivo*.
315 Muc2 is the major gel-forming mucus protein expressed in goblet cells and secretory
316 lineage cells in the SI[40]. IL22Fc-treatment increased the abundance of mucus and Muc2 protein
317 in luminal contents (Fig. 6ij). Expression of glycosyltransferases, including *Mgat4c*, and *Fut2*
318 were also induced by IL22Fc-treatment, as well by *V. cholerae* infection (Extended Data Fig.
319 10ab). Furthermore, modification of secreted Muc2 with fucose and *N*-acetylglucosamine was
320 elevated in treated mice (Extended Data Fig. 10c). Thus, IL22Fc administration elevates the
321 abundance of the Muc2+ cell population, as well as Muc2 secretion and modification.
322 To investigate if Muc2 plays a role in IL22 treatment mediated resistance to *V. cholerae*
323 colonization, we compared the effects of IL22Fc administration on *V. cholerae* colonization in
324 Muc2$^{-/-}$ and control (Muc2$^{+/+}$ or Muc2$^{+/-}$) littermates. Without IL22Fc administration, *V. cholerae*
325 colonization in Muc2$^{-/-}$ mice was comparable to that in control, with a modestly greater burden
326 (2.4-fold) in the distal SI of Muc2$^{-/-}$ mice. However, administration of IL22Fc had a much more
327 potent effect limiting *V. cholerae* colonization in both the proximal and distal SI in control vs
328 Muc2$^{-/-}$ mice; the Muc2$^{-/-}$ animals had a 817-fold (geometric mean) greater *V. cholerae* burden in
329 the proximal SI and 146-fold greater *V. cholerae* burden in the distal SI than control littermates
330 (Fig. 6k), suggesting that Muc2 contributes to the therapeutic activity of IL22Fc. Interestingly,
331 the role of Muc2 in mediating the activity of IL22Fc appears to be primarily in limiting the
332 pathogen's capacity to establish a colonization niche in the intestine (i.e., its founding population
333 size) rather than its proliferation (CFU/Ns) (Fig. 6lm). Since the Tn-seq screen (Fig.4a-c)
334 suggested that *V. cholerae* motility becomes more important for colonization in IL22Fc-treated
335 animals, we tested whether Muc2 impedes motility-dependent colonization. For these
336 experiments, competition assays in IL22Fc-treated Muc2$^{-/-}$ mice were used to compare
337 colonization of WT and motility-deficient strains *(ΔfliI*, *ΔfliD,* and *ΔmotB*). In marked contrast to
338 observations in Muc2$^{+/-}$ littermate controls, where the motility-deficient strains had a
339 colonization defect, the motility-deficient strains colonized Muc2$^{-/-}$ as well as WT *V. cholerae*
340 (Fig. 6n). Thus, the increased importance of flagellar-based motility for *V. cholerae* colonization
341 in IL22Fc-treated animals (Fig. 4) is likely attributable to this cytokine's stimulation of Muc2
342 production, which impedes pathogen access to its preferred niche along the epithelium in the
343 crypts.
344
345 **Discussion**
346 Given the extreme rapidity of cholera progression, innate defenses are particularly critical
347 for protecting humans against *V. cholerae*. Here, scRNA-seq profiling of epithelial and lamina
348 propria immune cell responses to experimental cholera in infant mice uncovered new facets of
349 mucosal defense in the small intestine and suggested that IL22-dependent mechanisms play a
350 role in cholera defense. IL22 therapy was highly protective against *V. cholerae* colonization and
351 diarrhea in infant mice. scRNA-seq profiling of IL22-treated animals offered new insights into
352 the mechanisms of this cytokine and uncovered an IL22-stimulated shift in the pattern of
353 intestinal epithelial cell differentiation toward the secretory cell lineage. The products of these
354 cells, including Muc2, appear to be critical for IL22-mediated protection from experimental

355 cholera, a mechanism that may generally contribute to the therapeutic effects of IL22 (Extended
356 Data Fig. 10d).
357 *V. cholerae* triggered changes in gene expression in most epithelial cell subsets but
358 unexpectedly increased the abundance of an enterocyte subset (cluster 5) whose signature gene
359 program was largely linked to defense. Since P5 mice lack Paneth cells, which are rich in
360 antimicrobial peptides and are thought to protect the crypt stem cells[14], cluster 5 enterocytes may
361 function in an analogous fashion during early life before Paneth cells arise around P15[14].
362 However, in contrast to Paneth cells, whose relative abundance undergoes a modest increase
363 during acute infection[41], the abundance of cluster 5 enterocytes cells increased >10-fold during
364 the 20 hours of exposure to *V. cholerae*. Because *V. cholerae* primarily localizes near the base of
365 villi[15], our findings raise the possibility that a consequence of the pathogen's presence in the
366 crypts is an alteration of the transcriptional program of adjacent enterocytes into this mucosal
367 defense-associated epithelial subset. *V. cholerae* preferentially colonizes in the distal SI[15,42] (Fig.
368 3bc). This localization may also explain why the epithelial and immune response is generally
369 more pronounced in this part of the SI.
370 Several studies have revealed that IL22 deficient mice have heightened susceptibility to
371 death from mucosal pathogens[21–23]. This work has led to the idea that IL22 promotes the integrity
372 of the epithelium through a variety of mechanisms, including increases in antimicrobial
373 proteins[22], epithelial cell surface modifications[27,43], and Paneth cell differentiation[35]. For enteric
374 pathogens, such as *C. rodentium* and *C. difficile*, experimental infections in IL22-/- mice have
375 not revealed marked increases in intestinal pathogen burdens[22,23,44], and heightened mortality has
376 been attributed to dissemination of intestinal bacteria, at least in part due to reduced activity of
377 complement C3[23]. Fewer studies have examined the consequences and the mechanisms of IL22
378 administration on pathogen burden. In adult mice *C. rodentium* infection, prophylactic
379 administration of IL22Fc only modestly reduces colonic colonization, but significantly reduces
380 disease by preventing epithelial damage[45].
381 In contrast, administration of IL22Fc almost entirely ablated the susceptibility of P5 mice
382 to *V. cholerae* colonization. Several IL22-dependent mechanisms likely account for the marked
383 reduction of *V. cholerae* colonization in IL22Fc-treated animals. Although there was a modest
384 benefit to administering IL22Fc after infection, the most dramatic therapeutic effects of IL22Fc
385 required that the cytokine be administered 24-48 hours before pathogen inoculation, indicating
386 that time is required for the beneficial effects of IL22Fc to accrue. IL22Fc stimulated alterations
387 in the transcriptional profile, cellular composition and even the length of the SI in P5 animals.
388 One of the striking changes elicited by IL22Fc administration was the augmentation in
389 expression of antimicrobial genes in most enterocyte subsets. For example, Reg3β became
390 detectable in epithelial cells throughout the crypt-villus axis. However, since we found that the
391 absence of Reg3β, in Reg3$\beta^{-/-}$ animals, did not render mice more susceptible to *V. cholerae*
392 colonization, physiologic levels of Reg proteins may be insufficient to impede colonization.
393 Instead, the supraphysiologic levels of Reg3β proteins and potentially other antimicrobial
394 products induced by IL22Fc treatment likely are important for the beneficial effects of IL22.
395 Similarly, IL22Fc administration markedly diminished colonic colonization with *C. rodentium* in
396 infant mice (Extended Data Fig. 6h), even though Reg3$\beta^{-/-}$ and Reg3$\gamma^{-/-}$ mice do not exhibit
397 elevated pathogen burden or disease severity associated with this pathogen in an adult mouse
398 model[44,46].
399 Although elevated Reg3β contributes to IL22Fc-mediated protection, our data suggests
400 that the major mechanism underlying reduced *V. cholerae* colonization in IL22Fc-treated

401 animals is due to elevated Muc2 production. IL22Fc administration appears to drive the
402 differentiation of stem cells towards production of secretory cells *in vivo*, as suggested in
403 organoids[36]. Studies in suckling Muc2$^{-/-}$ mice revealed that IL22Fc administration was not nearly
404 as potent at impeding *V. cholerae* intestinal colonization as in littermate Muc2$^{+/-}$ controls. Thus,
405 mucin production appears to be required for robust IL22Fc activity. We propose that the increase
406 in goblet cell number and Muc2 secretion in IL22Fc treated animals blocks the pathogen from
407 reaching its preferred niche, where it establishes a founding population in close apposition to the
408 epithelium of the crypt[42,47]. The IL22Fc-stimulated impedance of pathogen access to the
409 epithelium and crypts were apparent in the results of our TnSeq screen (Fig. 4). Moreover, the
410 competitive advantage of motility for colonization in IL22Fc-treated animals was not observed in
411 Muc2$^{-/-}$ mice (Fig. 6n), demonstrating the linkage between mucus-mediated protection and *V.*
412 *cholerae* motility. Glycosylation of Muc2 may also modulate disease outcome by reducing
413 cholera toxin expression[48]. Finally, since mucus is decorated with glycans and antimicrobial
414 proteins, and their functions are entwined[49], the dramatic beneficial effects of IL22Fc on
415 experimental cholera likely derive from synergistic interactions between these components of
416 innate intestinal defense. Overall, the marked reduction in *V. cholerae* colonization likely explain
417 the IL22Fc-mediated protection from cholera-like death in suckling mice.
418 Given the dramatic benefits of IL22Fc in the suckling mouse model of cholera and the
419 emergence of highly antibiotic-resistant *V. cholerae*[50], studies of this fusion protein as a
420 prophylactic agent for individuals susceptible to household contact infection[51] and/or as an
421 adjunctive therapy along with fluid resuscitation for cholera should be considered. Moreover,
422 IL22Fc administration may be an important therapeutic adjuvant for other extracellular enteric
423 pathogens such as enterotoxigenic *E. coli,* another pathogen that like *V. cholerae*, does not
424 damage the epithelium. However, several issues could complicate the translation of our findings
425 to humans. First, although infant mice represent an outstanding model for studies of *V. cholerae*
426 intestinal colonization[13] , these animals differ from humans in several important regards. For
427 example, human Paneth cells develop during embryogenesis, whereas mouse Paneth cells
428 develop around postnatal day 14[39,52,53]. Furthermore, the mechanisms by which IL22 protects the
429 host from infection may differ according to age, since IL22Fc administration did not elevate
430 goblet cell numbers in adult mice[35] unlike our findings in infant mice. Variations in epithelial
431 maturation, including the expression levels of IL22RA1/IL10RB, the IL22 receptor, in small
432 intestinal epithelial cells could impact on the efficacy of IL22Fc.
433 Despite these limitations, several clinical trials have already revealed the safety of
434 IL22Fc in humans. The primary dose-limiting adverse events when IL22Fc was administered
435 repeatedly were dermatologic[28,54,55]. Many additional studies, including whether IL22Fc
436 administration would be beneficial in the epidemiologic conditions, such as undernutrition where
437 cholera is prevalent, will be necessary to establish the safety of IL22Fc in relevant populations.
438 Costs of this fusion protein could be prohibitive but alternative cheaper methods to promote
439 endogenous IL22 production such as tryptophan metabolites that promote ILC3 differentiation
440 and IL22 production[56] may be feasible.
441

Materials and Methods

Mice

C57BL/6NCrl (strain code: 027) dams with infant mice (P3-P4) were purchased from Charles River Laboratory or bred in the Bio Safety Level 1 (BSL1) animal facility in Brigham and Women's Hospital. ROSA26LSL-TdTomato (B6.Cg-Gt(ROSA)26Sortm9(CAG-tdTomato)Hze/J; RRID:IMSR_JAX:007909), Lgr5-EGFP-IRES-creERT2 (B6.129P2-Lgr5tm1(cre/ERT2)Cle/J; RRID:IMSR_JAX:008875), IL22 knockout (C57BL/6-Il22tm1.1(icre)Stck/J; RRID:IMSR_JAX:027524) mice were from Jackson Laboratory (Bar Harbor, ME), *Atoh1*$^{Cre(ER\text{-}T2)}$ mice were a kind gift from Mikio Hoshino[57], and Muc2 knockout mice are gift from Anna Velcich[58]. Reg3β knockout (C57BL/6NCrl-Reg3bem1(IMPC)Mbp/Mmucd, RRID:MMRRC_067360-UCD) was obtained from the Mutant Mouse Resource and Research Center (MMRRC) at University of California at Davis, an NIH-funded strain repository, and was donated to the MMRRC by Kent Lloyd, D.V.M., University of California, Davis.

Mice were maintained in a BSL1 animal facility at Harvard Medical School or Brigham and Women's Hospital and transferred to the BSL2 animal facility for the infection experiments. Animals were maintained in cages filled with pine wood bedding and paper nesting material with chow (LabDiet 5053) and water by the animal facility staff. All animal experiments were performed according to protocols reviewed and approved by the Brigham and Women's Hospital Institutional Animal Care and Use Committee (protocol 2016N000416) and in compliance with the Guide for the Care and Use of Laboratory Animals. Both male and female mice were mixed and randomly assigned to experimental groups.

Bacteria Strains and culture

A *Vibrio cholerae* O1 Ogawa clinical isolate from the 2010 Haiti outbreak (HaitiWT)[59] was used here. Motility deficient mutants *(ΔmotB, ΔflgD, ΔfliI*) were created using homologous recombination as described[60]. To create targeting vectors, 1000 bp of DNA flanking each side of the targeted genes were amplified with Phusion DNA polymerase (NEB) and these segments were cloned into pCVD442's SmaI site using NEBuilder HiFi DNA assembly kit (NEB). Barcoded WT or motility deficient mutants *V. cholerae* were generated as previously described[61]. Fluorescent protein tdTomato labeled HaitiWT was created previously[62]. Primers used for the plasmid construction are listed in supplementary data (Supplementary Table S8). A streptomycin resistant isolate of *Citrobacter rodentium* strain ICC168 and *Salmonella Enterica* Serovar Typhimurium SL1344 strain were also used.

In vivo infection and colony forming unit (CFU) counting

V. cholerae was cultured in lysogeny broth (LB) with streptomycin (Strep) 200 μg/mL at 37 °C overnight (~18 h) prior to animal experiments. Mice at postnatal day 5 (P5) (2.5-3.5 g of body weight) were infected with $1x10^5$ Vc^{STAMP} by oral gavage using PE-10 tubing. Weight and survival were monitored every 4-8 hours. and animals were euthanized when they lost 20% of body weight. 3 cm of proximal SI (samples were dissected after the gastro-duodenal junction) and distal SI (~3 cm from the end of the ileum) were homogenized with stainless beads in 33% glycerol LB. The homogenates were serially diluted and plated on LB Strep agar plates for CFU counting.

C. rodentium was cultured in LB media containing 200 μg/mL strep at 37 °C overnight (~24 h). P5 infant mice were infected with $1x10^8$ cells of *C. rodentium* by oral gavage using PE-

488 10 tubing. Whole SI, and colon were dissected and homogenized in PBS and serial dilutions of
489 the tissue homogenates were plated on LB Strep agar plates for CFU counting.
490 *S.* Typhimurium was cultured in LB Strep 200 μg/mL at 37 °C overnight prior to animal
491 experiments. P5 infant mice were infected with $1x10^7$ cells of *S.* Typhimurium by oral gavage
492 using PE-10 tubing. Infant mice were euthanized 1- or 3-days post infection. Whole SI, colon,
493 liver, and spleen were dissected and homogenized in PBS, and serial dilutions of the tissue
494 homogenates were plated on LB Strep agar plates for CFU counting.
495
496 **CD45+ immune cell isolation from small intestine lamina propria**
497 Infant mice were euthanized with isoflurane. Three centimeters of the proximal and distal
498 SI, as described above, were collected, cut open longitudinally, and stored separately in buffer
499 [2% Fetal Bovine Serum (FBS), 50 μg/mL Gentamicin (Gen), Penicillin-Streptomycin (PS)
500 PBS] on ice until all animals were dissected. Tissues were incubated in 10 mL of reducing buffer
501 [10 mM DTT 10 mM HEPES 2% FBS, 50 μg/mL Gen, PS, RPMI 1640], for 10 min on ice,
502 followed by incubation in 10 mL of epithelial dissociation buffer [5 mM EDTA, 10 mM HEPES,
503 2% FBS RPMI1640] at 37°C for 25 min. The remained tissue was washed in PBS, cut into small
504 pieces using dissection scissors, and incubated in digestion buffer [0.5 mg/mL collagenase D, 0.3
505 mg/mL Dispase II, 0.05 mg/mL DNase I, 10 mM HEPES 5% FBS, RPMI 1640] at 37°C for 30
506 min. After vortexing for 20 sec, dissociated tissue was passed through a 40 μm filter and
507 centrifuged at 300 xg for 5 min. The immune cells were further separated in a 40% /80% Percoll
508 gradient by centrifugation at 1900 xg for 30 min. The layer between 40% and 80% Percoll was
509 collected, mixed with 2% FBS 2mM EDTA PBS, and centrifuged at 300 xg for 5 min. Cells
510 were resuspended in 2% FBS 2mM EDTA PBS containing anti-CD16/32 antibody, and stained
511 with anti-CD45 FITC antibody. After being washed in 2% FBS 2mM EDTA PBS, cells were
512 stained with propidium iodide before sorting, and the CD45+ PI- population was isolated using a
513 cell sorter (SH800Z, Sony, Japan).
514
515 **Single-cell isolation of Epcam+ epithelial cell**
516 Infant mice were orally infected with 10^5 WT *V. cholerae* cells and euthanized 20 hpi.
517 For IL22Fc (Genentech)[28] treatment, P4 mice were administered 20 μg of IL22Fc
518 intraperitoneally and returned to their dam. After 36 hours, the mice were euthanized. Proximal
519 and distal SI were collected, cut open longitudinally, and washed in Gut wash media [2% FBS,
520 10 mM HEPES, 100 μg/mL Pen/Strep, 50 μg/mL gentamicin in RPMI1640] in 15 mL conical
521 tubes. Tissues were rinsed in ice-cold PBS, incubated in Epithelial dissociation solution [30 mM
522 EDTA in PBS] on-ice for 40 min, shaken gently 30 times every 5 min, and then vortexed for 20
523 seconds. Tissue pieces were removed with forceps. Dissociated cells in the supernatant were
524 centrifuged and resuspended in ice-cold PBS. This step was repeated twice to wash out EDTA.
525 The cell pellets were resuspended in Dispase solution [2% FBS, 0.1 mg/mL dispase in 4 mL
526 RPMI1640 per animal] at RT for 3-5 min, then cells were dissociated by pipetting with a wide-
527 bore tip, followed by pipetting 10 times with normal tips. 4 mL of ice-cold RPMI1640
528 containing 2% FBS was added to the cell suspension and filtered through a 70 μm cell strainer.
529 The strainer was washed with ice-cold RPMI1640 containing 2% FBS to collect the cells. Cells
530 were pelleted by centrifugation, stained with anti-Epcam FITC (1:100), and passed through a 100
531 mm cell strainer. After being stained with LIVE/DEAD Fixable Violet Dead cell staining kit
532 (ThermoFisher, L34964), live Epcam+ cells were sorted by a SONY SH800Z Cell sorter.
533

534 **Single-cell RNA-Seq**

535 Sorted CD45+ SI lamina propria (LP) immune cells or Epcam+ epithelial cells were
536 collected into PBS containing 2% FBS, followed by centrifugation at 1000 xg for 5 min,
537 resuspended in PBS, counted, and passed through a 40 μm cell strainer. Single-cell suspensions
538 were applied to a 10X Chromium Controller for GEM generation using Chromium Next GEM
539 Single Cell 3' Reagent Kits v3.1 (10x Genomics). After barcoded cDNA generation, samples
540 were amplified with the index primers (Dual Index Kit TT Set A, 10x Genomics) for 12 cycles.
541 The libraries were sequenced on a NovaSeq 6000 S1 or NextSeq500. Data analysis was
542 performed using 10x Cloud Analysis, and the filtered feature H5 files were used for further
543 analysis with the Seurat package in R. Seurat objects were generated using Seurat v5.0.0
544 (https://satijalab.org/seurat/). Low-quality droplets (nFeature_RNA > 200 & nCount_RNA >
545 1000 & percent.mt < 20) and potential multiplets detected by scDblFinder were removed. Data
546 from uninfected and infected proximal and distal SI samples were normalized by SCTransform
547 (method = "glmGamPoi", vst.flavor = "v2") and integrated by Seurat's functions. Clustering was
548 performed with Seurat's FindCluster (dims = 1:30, resolution = 0.4 for epithelial, 1.0 for CD45+
549 cells). Marker genes and differential gene expression analysis on each cell cluster was performed
550 using the FindMarkers function of Seurat, and we annotated clusters based on canonical marker
551 genes. Single-cell pathway analysis (SCPA) was performed by SCPA package v1.6.1 with
552 default settings (downsample = 500, min_genes = 15, max_genes = 500) for epithelial cells, and
553 downsample = 300 for CD45+ immune cells. Pathway enrichment was obtained by multiplying -
554 1 to the fold change in the SCPA output. Pathways containing the following words were selected
555 for coloring in Fig.1d: "INTERFERON" for IFN; "TNFA", "INFLAMMATORY",
556 "INFLAMMATION" for TNFα, Inflammatory; "M_PHASE", "S_PHASE", "PRO_PHASE",
557 "ANAPHASE", "CHROMATIDS", "G2_M_CHECKPOINTS", "SYNTHESIS_OF_DNA",
558 "MITOTIC", "DNA_REPLICATION", "MYC", "E2F" for Mitosis; "TRANSLATION",
559 "RIBOSOME", "RIBOSOMAL" for Translation and Ribosome; "GOLGI", "MTORC",
560 "UNFOLDED", "HYPOXIA" for Golgi, ER, mTOR; "AMINO_ACID", "AMINO_ACIDS",
561 "FATTY_ACID", "OXIDATIVE_PHOSPHORYLATION", "TCA_CYCLE" for Metabolism.
562 For Fig.2b: "INTERFERON" for IFN; "IL17", "IL23", "PROINFLAMMATORY" for
563 Proinflammatory, IL17, IL23; "TRANSLATION", "RIBOSOME", "RIBOSOMAL" for
564 Translation, Ribosome; "GOLGI", "UNFOLDED", "MTOR", "HYPOXIA" for Golgi, ER, and
565 mTOR. For Extended Data Fig.7e: "ANTIMICRO" for Antimicrobial peptides; "M_PHASE",
566 "S_PHASE", "PRO_PHASE", "ANAPHASE", "CHROMATIDS", "G2_M_CHECKPOINTS",
567 "SYNTHESIS_OF_DNA", "MITOTIC", "DNA_REPLICATION" for Mitosis;
568 "TRANSLATION", "RIBOSOME", "RIBOSOMAL" for Translation and Ribosome; "E2F" for
569 E2F; "MYC_" for MYC Target; "AMINO_ACID", "AMINO_ACIDS", "LIPID", "GLUCOSE",
570 "SUGAR", "FATTY" for Lipid, Sugar, Amino acid. HALLMARK and KEGG pathways
571 containing the following words were plotted in Extended Data Fig. 2c: "AMINO_ACID",
572 "AMINO_ACIDS", "FATTY_ACID", "OXIDATIVE_PHOSPHORYLATION",
573 "TCA_CYCLE".

574 In RNA velocity analysis, *V. cholerae*-infected intestinal epithelial cells scRNA-seq data
575 were processed using Cell Ranger, velocyto, Seurat and scVelo, according to the scVelo
576 instruction (https://scvelo.readthedocs.io/en/stable/index.html). Briefly, spliced and unspliced
577 transcript counts were quantified from Cell Ranger output using velocyto[63] (v0.17.17) with the
578 mouse reference genome (mm10). To maintain consistency with our prior single-cell analysis,
579 velocity data was integrated with the Seurat (v5)-processed dataset. Cell barcodes from velocyto

loom files were matched to the quality-controlled Seurat object (after doublet removal and QC filtering). Pre-computed UMAP coordinates and cluster annotations from the Seurat SCTransform/RPCA integration workflow were imported into the scVelo analysis framework, ensuring identical cell embeddings between the two analyses. RNA velocity was estimated using scVelo[64] (v0.3.0) in Python (v3.10) and velocity streamlines were projected onto the UMAP embedding to visualize cellular state transitions.

Cell-cell communication analysis between epithelial and immune cells were performed using the CellChat[20] (v2.2.0). First, epithelial and immune cell single cell RNA-seq data were integrated according to condition (uninfected or infected). Cellchat objects were generated using createCellChat function. Comparison of the communication probabilities mediated by ligand-receptor pairs from LTi-like ILC3 to enterocytes were performed by netVisual_bubble function and visualized by netVisual_chord_gene function with default settings.

Flow cytometry

SI lamina propria cells were isolated according to the protocol above. For intraepithelial lymphocyte (IEL) isolation, distal SI tissue were cut open longitudinally and incubated in 10 mL of reducing buffer [10 mM DTT 10 mM HEPES 2% FBS, 50 μg/mL Gen, PS, RPMI 1640], for 10 min on ice, followed by incubation in 10 mL of epithelial dissociation buffer [5 mM EDTA, 10 mM HEPES, 2% FBS RPMI1640] at 37°C for 25 min. After removal of the remaining tissue pieces by pipetting, supernatants were passed through a 70 μm cell strainer and spun down at 300 xg for 5 min. The pellets were resuspended in 2 mL FACS buffer and overlayed onto 40%/80% Percoll gradients. Cells accumulated between 40% and 80% Percoll were transferred to new tubes, washed in 5 mL of FACS buffer, and centrifuged at 500 xg for 5 min. Cell pellets were washed in 2% RPMI1640 media and used for cell culture.

Cells isolated from LP and IEL were cultured in 10 % FBS RPMI1640 supplemented with 1x Brefeldin A (Biolegend) and Penicillin/Streptomycin (Gibco) for 3 h. Cells were mixed with anti-CD16/32 antibody (Biolegend, 101302) to block Fc binding, and stained with the following combination of antibodies in 2% FBS 2mM EDTA PBS; Live/Dead Aqua (ThermoFisher, L34957), anti-CD45+ Alexa Fluor 700 (BD Biosciences, 560510), anti-CD3e Super Bright 600 (ThermoFisher, 63-0031-82), anti-B220 FITC (Biolegend, 103206), anti-CD11b FITC (Biolegend, 101206), anti-CD11c FITC (BD Biosciences, 557400), anti-TCRγ/δ APC (Biolegend, 118143). After 30 min incubation at room temperature, cells were washed in 2% FBS 2mM EDTA PBS and fixed in Fixation/ Permeabilization solution (ThermoFisher, 88-8824-00) at 4 °C overnight. After washing, cells were stained with anti-IL22-PerCP-eFluor710 (ThermoFisher, 46-7222-80) at room temperature for 30 min and analyzed using a Cytek Northern Light (Cytek, MA).

Immunohistochemistry

Distal small intestines were fixed in 4% paraformaldehyde (PFA) PBS for 4 hours and dehydrated in 20% sucrose-PBS overnight. Tissue was embedded in OCT Compound: 20% sucrose-PBS = 2.5:1 and frozen by liquid nitrogen. Tissue blocks were cut into 10 μm sections with a cryostat at -18 °C (Leica) and the sections were dried at room temperature for 2h and stored at -80 °C until use. Tissue sections were washed in PBS, blocked in blocking buffer [5% goat serum 0.1% Triton X100 PBS] for 30 min, and stained with sheep anti-Reg3β antibody (1:100, R&D Systems), rabbit anti-*V. cholerae* antisera Ogawa (1:100, BD Difco) at 4 °C overnight. Tissue sections were washed in PBS twice and stained with anti-sheep IgG Alexa

626 Flour 555 (1:200, ThermoFisher), goat anti-rabbit IgG Alexa Flour 488 (1:200, ThermoFisher),
627 or chicken anti-rabbit IgG Alexa Flour 647 (1:200, ThermoFisher) and DAPI (1:1000,
628 ThermoFisher) at room temperature for 30 min. The sections were washed in PBS and covered
629 with Prolong gold antifade reagent (ThermoFisher).
630 For PAS staining for paraffin sections, fixed tissue was processed, sectioned, and stained
631 at the Harvard Rodent Histology core. For Muc2 staining, paraffin sections were deparaffinized
632 with xylene for 10 min x2, rehydrated in 100%, 80%, 70%, 60% ethanol, and PBS for 5 min in
633 each solution. Sections were incubated with antigen retrieval buffer (citrate buffer, pH 6.0) and
634 microwaved for 10 min. Rehydrated tissue was blocked in blocking buffer for 30 min, stained
635 with rabbit anti-Muc2 antibody (1:100, Proteintech) in blocking buffer overnight, washed in
636 PBS, and stained with anti-rabbit IgG Alexa Flour 488 (1:200, ThermoFisher) at room
637 temperature for 30 min. The tissue was stained with DAPI, washed in PBS, and mounted in
638 Prolong gold antifade reagent (ThermoFisher, P36934).
639 Fluorescent and PAS stain images were imaged with a Nikon Eclipse microscope with a Nikon
640 Microscope Objective Plan Apo l 20x/0.75 OFN25 DIC N2 lens, Plan Flour 40x/1.30 Oil lens, or
641 Plan Apo VC 100x/1.40 Oil DIC lens (Nikon) and captured with a Andor iXon DU-897E-CS0-
642 #BV-500 Camera (Oxford Instruments).
643
644 **Single molecule RNA Fluorescence *in situ* hybridization (RNAScope)**
645 For detection of *Fgb* and *Sult6b2*, the dissected distal SI tissue was fixed in 4% PFA-PBS
646 overnight at 4°C and dehydrated in 20% Sucrose-PBS overnight. Tissue was embedded in OCT
647 Compound: 20% sucrose-PBS = 2.5:1 and frozen by liquid nitrogen. Tissue blocks were cut into
648 10 μm sections with a cryostat at -20 °C (Leica). The sections were attached to MAS coated slide
649 glass (Matsunami), dried at -20°C for 2h and were stored at -80 °C until use. Tissue sections
650 were stained according to the manufacture's RNAScope protocol (ACDbio) with hybridization
651 probes: Mm-Sult6b2-C3 (1789851-C3) and Mm-Fgb-C2 (578921-C2). For detection of *Atoh1*
652 and *Spdef*, P4 infant animals were administered PBS or 20 μg of IL22 and were returned to their
653 dam. After 36 h, mice were euthanized, and tissues were processed as described above. Tissue
654 sections were stained with hybridization probes Mm-Atoh1 (408791) and Mm-Spdef-C2
655 (544421-C2). Stained sections were imaged using a Nikon Eclipse microscope as above.
656
657 **Proliferating cell staining with 5-ethynyl 2´-deoxyuridine (EdU)**
658 For the staining of *V. cholerae* infected animal tissues, P5 animals were randomly
659 assigned to receive 40 μg of EdU at 0 hpi or 18 hpi. The mice were infected with 10^5 cells of *V.*
660 *cholerae* and euthanized and dissected at 20 hpi. For the staining of IL22Fc-treated animal
661 tissues, P4 infant littermate mice were randomly assigned to receive either PBS or IL22Fc. Mice
662 were administered 40 μg of EdU and PBS or 20 μg of IL22Fc intraperitoneally and returned to
663 their dam. After 36 hours, the mice were euthanized and dissected. For both experiments, the SI
664 tissue was fixed, embedded, and cut into 10 μm cryosections as described above in methods for
665 Immunohistochemistry or RNAScope. After the immunohistochemistry or RNAScope staining
666 procedure, tissue sections were stained with Click-iT™ EdU Cell Proliferation Kit for Imaging,
667 Alexa Fluor™ 647 dye (ThermoFisher), according to the manufacture's protocol. Figure images
668 were captured with Nikon Eclipse microscope as above.
669
670 **Lineage tracing**

671 *Lgr5*$^{Cre(ER-T2)}$;*Rosa26R*$^{LSL-tdTomato}$ mice were given 200 μg of tamoxifen 9 hours before and
672 again at the same time as infection with 10^5 cells of *V. cholerae*. Mice were euthanized at 20 hpi.
673 The SI was fixed, embedded, and cut into 10 μm cryosections as described above (See
674 RNAScope). Tissue sections were stained with hybridization probes: Mm-Sult6b2-C3 (1789851-
675 C3) and Mm-Fgb-C2 (578921-C2) for RNAScope and further stained with anti-RFP antibody
676 (1:200, Rockland Immunochemicals, 600-401-379). After washing in PBS, tissue was stained
677 with chicken anti-rabbit IgG Alexa 647 (1:200, ThermoFisher, A-21443) for 30 min, stained with
678 DAPI (1:500) for 5 min, and mounted in Prolong Gold Antifade Reagent.
679 *Atoh1*$^{Cre(ER-T2)}$;*Rosa26R*$^{LSL-tdTomato}$ mice were given 200 μg of tamoxifen 9 hours before
680 and again at the same time as IL22Fc (20 μg), and euthanized 37 hours after IL22Fc
681 administration. The tissue was processed according to the protocol for immunohistochemistry
682 (See above). For Ki67 staining, rabbit anti-Ki67 antibody (1:100, Abcam, ab16667) and anti-
683 rabbit IgG Alexa 647 (1:200) were used. For mucus positive secretory lineage staining, tissue
684 section was stained with UEA-I FITC (1:100, vector), phalloidin Alexa 647 (1:200,
685 ThermoFisher), and DAPI (1:1000), for 10 min, washed in PBS, and mounted in Prolong Gold
686 Antifade Reagent. Figure images were captured with Nikon Eclipse microscope as above.
687
688 **iDISCO clearing and 3D imaging**
689 Two-centimeter pieces of distal small intestine were harvested from uninfected and
690 infected animals and fixed in 4% paraformaldehyde PBS at 4°C overnight. Tissues were washed
691 in PBS with 0.2% Tween-20 and 100 μg/mL Heparin for 1 hour twice and dehydrated gradually
692 in 20%, 50%, 80% methanol (in PBS) for 1h, and twice in 100% methanol for 1h. Samples were
693 then incubated overnight at room temperature on a shaker (50-60 rpm) in 66% Dichloromethane
694 (Sigma) /33% Methanol. Samples were then incubated with 5% H_2O_2 in 20% DMSO at 4'C
695 overnight, and then washed in 100% methanol, then 20% DMSO/methanol, and then rehydrated
696 with 80%, 60%, 50%, 40%, 20% methanol in PBS for 1h each, and PBS for 1h twice. Tissues
697 were then permeabilized in 0.2% Triton X-100 at RT for 1h, and 0.2% Triton X-100/20%
698 DMSO/0.3M Glycine for 1day at 37°C with gentle agitation. After being washed in PBS with
699 0.2% Tween-20 and Heparin (100 μg/ml) at RT for 1h twice, tissues were blocked in PBS with
700 0.2% TritonX-100/10% DMSO/6% Donkey Serum at 37°C with gentle agitation for 1 day,
701 stained with rat anti-IL22 (1;100. Thermofisher) in PBS with 0.2% TritonX-100/10% DMSO/3%
702 Donkey Serum at 4 °C for 2 days. The tissues were washed in wash buffer [PBS with
703 0.2%Tween-20, 100 μg/mL Heparin] for 30 min for 5 times, incubated with secondary antibody;
704 anti-rabbit IgG Alexa 647 (1:200, Invitrogen), anti-rat IgG Alexa 568 (1:200, Invitrogen), and
705 rabbit anti-Epcam Alexa 488 (1:100, Biolegend) in PBS with 0.2% TritonX-100/10% DMSO/6%
706 Donkey Serum at 37C for 1 day. Samples were washed in wash buffer for 5 times, stained with
707 2μg/mL DAPI in PBS, washed in wash buffer for 5 times. To clear the tissue, samples were
708 dehydrated with 20, 40, 50, 80, and 100% methanol and incubated in 66% DCM/33% methanol
709 at room temperature for 3 hours, subsequently incubated in 100% dichloromethane at room
710 temperature for 15 min twice, and incubated in 100% ethyl cinnamate. Tissues were placed on a
711 glass bottom dish, and covered with100% ethyl cinnamate. Three dimensional images were
712 captured using a confocal microscope (Stellaris 8 Falcon DIVA, Leica) with Fluotar 16x/0.6
713 multi-immersion lense, and LasX acquisition software, built with arivis Vision 4D software
714 version 4.1.2 (Zeiss).
715
716 **Quantitative PCR**

717 Distal SI tissue from animals uninfected or infected with WT *V. cholerae* was collected at
718 20 hpi and homogenized in Trizol (ThermoFisher) with a bead beater with 3.2 mm metal beads.
719 Total RNA was isolated according to the manufactures' protocol. Total RNA was used for One-
720 step cDNA synthesis and qPCR with the Luna Universal One-Step RT-qPCR Kit (NEB,
721 E3005L) according to the manufacture's protocol. The amplification signal was analyzed using a
722 StepOnePlus Real-Time PCR System (Applied Biosystems). qPCR primer pairs are listed in
723 Supplementary Table 8.
724
725 **Sequence tag-based analysis of microbial population dynamics (STAMP)**
726 Infant mice were orally infected with barcoded Vc^{STAMP} and 16-20 hours later sacrificed
727 and tissue homogenates were plated for CFU counting as described above. The remaining SI
728 homogenates were plated on large (15cm diameter) LB-streptomycin plates and after overnight
729 culture at 37°C, cells were collected in 33% glycerol LB and stored at -20 °C. Two microliter of
730 each cell suspension was diluted with 100 µL milliQ water and boiled at 95 °C for 15 min. Each
731 sample was amplified with One Taq DNA polymerase, forward and reverse primers with unique
732 sequences that enable samples to be distinguished were used. The amplicons were purified using
733 the Genejet PCR purification kit and sequenced with NextSeq P1 100 cycle Reagent Kit
734 (Illumina). The barcode sequences were analyzed with STAMPR pipeline as described[29].
735
736 **Transposon insertion sequence (Tn-seq)**
737 A Tn-seq library in *V. cholerae* strain HaitiWT was used[65]. The library contained
738 ~195,000 distinct transposon insertions. Animals were intraperitoneally administered PBS
739 (control; n = 3) or IL22Fc (n=4) 24 h prior to infection. The transposon library was cultured in
740 25 mL of LB liquid media containing 200 µg/mL streptomycin and 50 µg/mL Kanamycin
741 (Strep/Kan) for 3 h at 37 °C with shaking. A higher inoculum size (~10^8 CFU) and lower dose of
742 IL22Fc (5 µg/animal) was used in these experiments compared to experiments described in Fig.3
743 to ensure that there would be sufficient numbers of CFU in intestinal homogenates to allow
744 statistically robust comparisons of the abundances of insertions in the inoculum with the
745 outputs[66] . Distal SI tissue was homogenized in 1mL of 33% glycerol LB and plated on LB
746 Strep/Kan agar plate and cultured at 37°C overnight. All colonies on those plates were harvested
747 in 2 mL of 33% glycerol LB and stored at -20°C until further processing. Genomic DNA
748 (gDNA) was extracted using gDNA extraction kit (Qiagen), sheared into 400 base pair (bp)
749 using Covaris, and was purified using the DNA clean kit (Qiagen). gDNA fragments were
750 repaired with Blunting enzyme mix (NEB), A-tails were added using Taq polymerase and dATP,
751 and ligated with adaptor sequences. Adaptor-ligated gDNA was amplified using Phusion PCR
752 polymerase with adaptor primers for 30 cycles. After purification, the amplicon was further
753 amplified with var primers and index barcodes. The amplified library with sizes between 300-
754 500 bp were isolated using SPRIselect beads (Beckman-Coulter). Sequencing was performed
755 using a Nextseq1000 with P1 100 cycle cartridge (illumina). Tn-seq data was analyzed using the
756 RTISAn pipeline as previously described[67].
757
758 **Competition assay with barcoded *V. cholerae***
759 Diluted WT or mutant *V. cholerae* STAMP libraries were cultured on 200 µg/mL
760 streptomycin LB (LB Strep) plates and 4-8 isolated colonies were picked. These single colonies
761 were then individually grown in LB Strep liquid media with shaking at 37 °C overnight; then

762 after adjusting OD600 to 1 with LB media, they were mixed in equal ratios. The barcoded strain
763 mix was stored as a glycerol stock at -80 °C until use.
764 P4 WT infant mice were used for Figure 4d. P4 Muc2$^{+/-}$ or Muc2$^{-/-}$ littermate were used
765 for Figure 6n. The mice were intraperitoneally administered PBS or 5 μg IL22Fc 24 hours before
766 infection. The barcoded strain mix was cultured in LB Strep liquid media with shaking at 37 °C
767 overnight and infant mice were orally inoculated with $1x10^7$ cells of the strain mix and sacrificed
768 at 20 hpi. Homogenates of the distal SI tissue were plated on LB Strep plates, grown at 37 °C
769 overnight, and colonies were collected in 33% glycerol LB. Genomic DNA was extracted from
770 the collected bacteria and DNA barcodes were analyzed according to the protocol described
771 above. To calculate competitive indices, the frequency of each barcode in the output population
772 (from intestinal homogenates) was divided by the frequency in the inoculum. The geometric
773 mean of the resultant ratio of barcode frequencies (output/inoculum) in mutants were compared
774 to those of the WT strain in each individual mouse.
775
776 **Reg3β bactericidal assay *in vitro* and *in vivo***
777 An overnight culture of wild type *V. cholerae* was inoculated in LB Strep and incubated
778 at 37°C for 3 hours. The cell density (OD600) was adjusted to 0.1 (~10^8 cells/mL) and cells were
779 washed in MES buffer (100mM MES pH5.8, 25mM NaCl) twice. 10^5 cells were mixed with
780 recombinant Reg3β protein (Sino Biological, 51153-M08H) in MES buffer and incubated at
781 37°C for 3 h. Cells were resuspended in LB media and either plated on LB Strep agar or growth
782 was monitored in a BioTek Epoc2 Microplate Spectrophotometer (Agilent, CA).
783 For *in vivo* assays, P5 infant animals were given 33.3ug of Reg3β protein orally 30 min
784 before and 1 hour after mice were orally gavaged with 10^5 cells of WT *V. cholerae*. Proximal
785 and distal SI tissues were harvested and homogenized in 33% glycerol LB at 16 hours post
786 infection. Serial dilutions of tissue homogenates were plated on LB Strep plates for CFU
787 counting.
788
789 **Image analysis**
790 All images were analyzed using Fiji Software version 2.14.0
791 (https://imagej.net/software/fiji/).
792 Pearson's correlation coefficient of colocalization between Reg3β and *V. cholerae* were analyzed
793 using Coloc2 plugin (https://github.com/fiji/Colocalisation_Analysis). Z-stack images (0.3μm
794 distance per image) of colocalization between Reg3β and *V. cholerae* were captured with Nikon
795 Microscope Objective Plan Apo VC 100x/1.40 Oil DIC lens and 3D images were built using 3D
796 viewer plugin (https://github.com/fiji/3D_Viewer). *Atoh1*+, *Spdef*+, and EdU+ cells were
797 counted using Find Maxima function with the same setting of Prominence across all compared
798 images.
799
800 **Protein extraction, digestion, LC-MS/MS acquisition, and data analysis**
801 The distal SI tissue was collected from control or IL22Fc-treated infant animals and cut
802 open longitudinally. The tissue was incubated in 4 mL of wash buffer [1mM DTT PBS with
803 protease inhibitor (Roche, 4693159001)] on ice for 10 min and vortexed for 20 seconds. After
804 the removal of tissue pieces, intestinal washes were centrifuged at 100 xg for 1 min to remove
805 the large pieces of intestinal contents. The supernatant was concentrated by centrifugation at
806 4000 xg with 3 kDa MWCO Amicon Ultra centrifugal filter unit for 1 hour. The volume of the
807 concentrate was adjusted to 400 μL with wash buffer. The supernatants were processed for LC-

808 MS/MS analysis using the ENRICH-iST kit (PreOmics, #P.O.00163). Assay details have been
809 described previously[68], including protein enrichment, denaturation, reduction, alkylation,
810 enzymatic digestion, and peptide cleanup within a single workflow. Briefly, mucus proteins were
811 captured on paramagnetic enrichment beads in binding buffer, followed by multiple bead-based
812 wash steps to remove salts, lipids, and low-molecular-weight contaminants. Bead-captured
813 proteins were denatured, reduced, and alkylated using the supplied lysis buffer at elevated
814 temperature and digested on-bead with a Trypsin/LysC protease mixture. Digestion was
815 terminated by stop solution, and peptides were purified using the solid-phase extraction cartridge
816 with sequential washes to remove impurities. Peptides were eluted in volatile buffer, dried
817 completely by vacuum centrifugation (SpeedVac SPD120), and stored at −80 °C until LC-
818 MS/MS analysis.
819 Peptides were reconstituted in 5-10 µL of solvent A (2.5% acetonitrile, 0.1% formic acid)
820 and separated by nano-scale reverse-phase liquid chromatography using a custom-packed
821 capillary column (100 µm inner diameter × ~30 cm length) containing 2.6 µm C18 spherical
822 silica beads and terminated with a flame-drawn electrospray tip[69]. Subsequently, peptides were
823 loaded via an autosampler and eluted using a linear gradient of increasing concentrations of
824 solvent B (97.5% acetonitrile, 0.1% formic acid). Eluting peptides were ionized by electrospray
825 and analyzed on an Orbitrap Velos Pro hybrid ion trap-Orbitrap mass spectrometer (Thermo
826 Fisher Scientific).
827 MS raw files were searched against the UniProt FASTA databases using Sequest
828 (Thermo Fisher Scientific)[70]. Databases included reversed (decoy) sequences to enable
829 estimation of false discovery rates. Peptide-spectrum matches were filtered to achieve a peptide-
830 level false discovery rate of 1–2%. Carbamidomethylation of cysteine residues was specified as a
831 fixed modification during database searching. Enzyme specificity was defined as cleavage at the
832 carboxyl terminus of arginine and lysine residues, consistent with digestion by trypsin and LysC.
833 A maximum of ## missed cleavages was allowed. All bioinformatic analyses were performed
834 using Perseus (version 2.0.7.0)[71,72] as well as standard analytical workflows implemented in R
835 (version 4.5.2).
836
837 **Immunoprecipitation and western blot for intestinal contents**
838 The distal SI tissue was collected from control or IL22Fc-treated infant animals and cut
839 open longitudinally. The tissue was incubated in 4 mL of wash buffer [1mM DTT PBS with
840 protease inhibitor (Roche, 4693159001)] on ice for 10 min and vortexed for 20 seconds. After
841 the removal of tissue pieces, intestinal washes were centrifuged at 100 xg for 1 min to remove
842 the large pieces of intestinal contents. The supernatant was concentrated by centrifugation at
843 4000 xg with 3 kDa MWCO Amicon Ultra centrifugal filter unit for 1 hour. The volume of the
844 concentrate was adjusted to 400 µL with wash buffer. Twenty microliter of intestinal wash was
845 used for immunoprecipitation and western blot. An antibody against Muc2 (ProteinTech, 27675-
846 1-AP) was mixed with Pierce Protein A/G Magnetic Beads (Pierce, 88802) in PBS for 1 hour
847 and further mixed with intestinal wash in 500 µL of IP buffer [0.1% Tween 20 PBS with
848 protease inhibitor] for 3 hours at 4 °C. Beads were washed in 1mL of IP buffer three times,
849 mixed with SDS-PAGE loading buffer containing DTT (NEB, B7703S), and boiled at 95 °C for
850 5 min. SDS-PAGE (ThermoFisher, WG1403BOX) and transferring to nitrocellulose membrane
851 (ThermoFisher. IB23001) were performed using iBlot 2 (ThermoFisher) according to
852 manufactures' protocol. After blocking the membrane with 5% skimmilk TBST, the membrane
853 was incubated with antibody against Muc2 (Abcam, EPR23479-47, 1:1000) in TBST at 4 °C

854 overnight. After wash in TBST, the membrane was incubated with IRDye 800CW goat anti-
855 rabbit IgG Secondary Antibody (LICORbio, 926-32211, 1:5000) and UEA-I Fluorescein (vector,
856 FL-1061, 1:5000) at room temperature for 1 hour. After wash in TBST, the fluorescent signal
857 was detected using ChemiDoc MP imaging system (Bio-rad).
858
859 **Statistical Analysis**
860 Statistical analysis was performed using Prism10 software version 10.4.0. For the CFU,
861 founding population (Ns), and CFU/Ns comparison in animal infection studies, values were
862 transformed to logarithm 10 before statistical analysis. n represents the number of animals unless
863 otherwise noted in the figure legend.
864
865 **Acknowledgments**
866 We thank members of the Waldor lab for helpful comments on this project and
867 manuscript, Franz Zingl Ph.D. for data in Fig. 5d, Krithika Badarinath for advice on lineage
868 tracing. We thank Paula Montero Llopis, Ph.D., Praju Vikas Anekal, Ph.D., and Adrienne Wells,
869 Ph.D. in the MicRoN Center at Harvard Medical School for histology, immunohistochemistry
870 and 3D imaging, the Harvard Rodent Histology Core for tissue sectioning and staining, the
871 Harvard Biopolymers facility for RNA sequencing, and the Harvard Research Computing Core
872 for providing the computational analysis platform. We are grateful to Anna Velcich at College of
873 Medicine/Albert Einstein Cancer Center for providing us Muc2 knockout mice, and to
874 Genentech for providing us IL22Fc recombinant protein.
875
876 **Funding:**
877 National Institutes of Health grants R01 AI042347 (M.K.W.), and R01 DK082889 (R.A.S.)
878 Howard Hughes Medical Institute (M.K.W.)
879
880 **Author contributions:**
881 Conceptualization: M.S., Y.H., H. Z., M.K.W.
882 Methodology: M.S., Y.H., H. Z., Z.L., G.T.
883 Investigation: M.S., Y.H., Z.L., G.T.
884 Visualization: M.S., Y.H., Z.L.
885 Funding acquisition: M.K.W.
886 Project administration: M.K.W.
887 Supervision: R.A.S., M.K.W.
888 Writing – original draft: M.S., Y.H., and M.K.W.
889 Writing – review & editing: M.S., Y.H., H.Z., Z.L., R.A.S., and M.K.W.
890 **Competing interests:** Authors declare there is no competing interests
891
892 **Licence information**
893 This article is subject to the Howard Hughes Medical Institute (HHMI)'s Open Access to
894 Publications policy. HHMI laboratory heads have previously granted a non-exclusive CC BY 4.0
895 licence to the public and a sublicensable licence to HHMI in their research articles. Pursuant to
896 those licences, the author-accepted manuscript of this article can be made freely available under
897 a CC BY 4.0 licence immediately upon publication. This article is the result of funding in whole
898 or in part by the National Institutes of Health (NIH). It is subject to the NIH Public Access
899 Policy. Through acceptance of this federal funding, the NIH has been given the right to make this

article publicly available in PubMed Central upon the Official Date of Publication, as defined by the NIH.

Data and materials availability:

The single-cell RNA sequence data have been deposited in the NCBI Gene Expression Omnibus (GEO) database under accession number GSE288380. The proteomics data have been deposited in Proteomics Identification database (PRIDE) under accession number XXX.

Supplementary Materials

Extended Data Fig.1 to 10

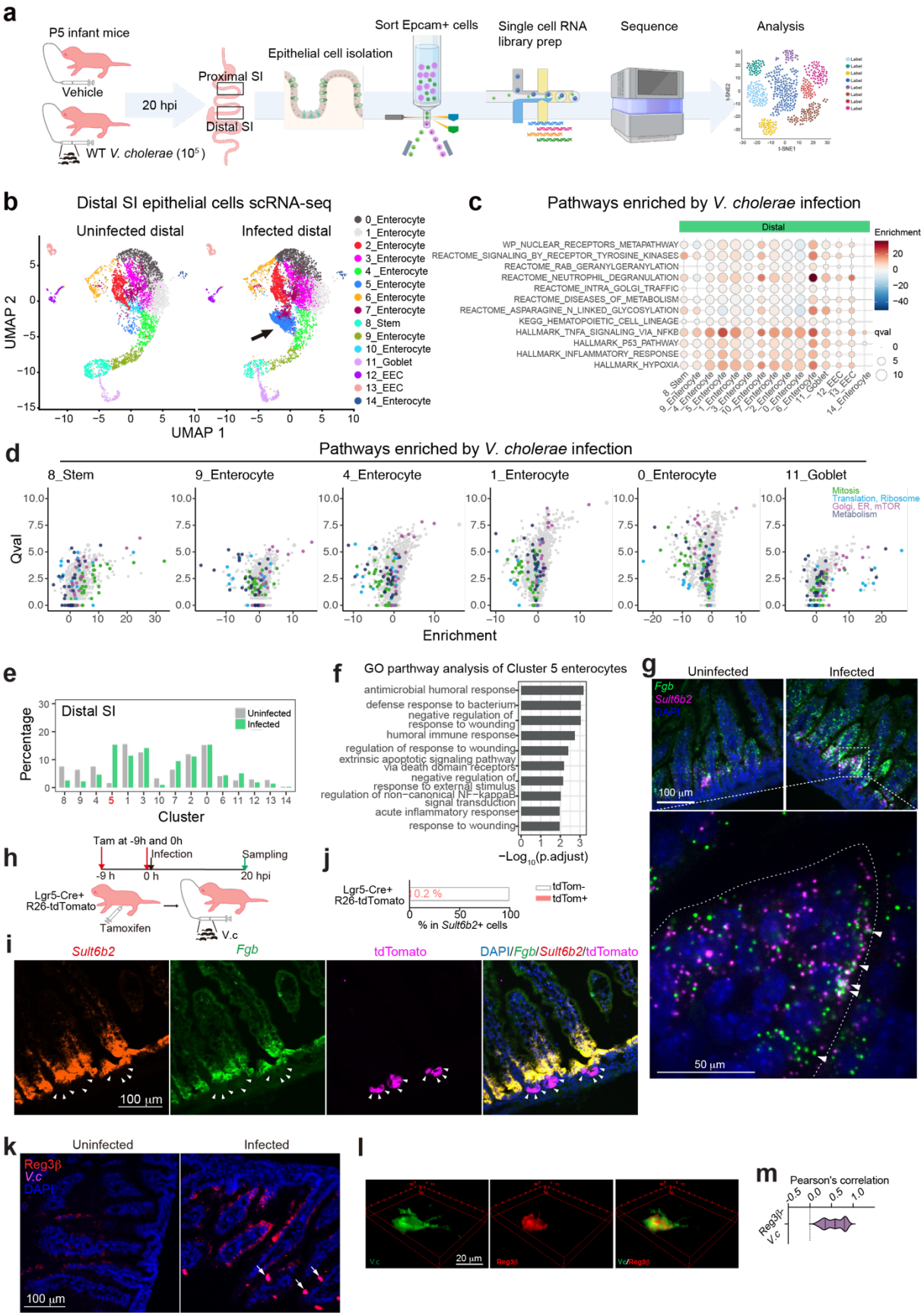
a
P5 infant mice
Vehicle
WT V. cholerae (10^5)
20 hpi
Proximal SI
Distal SI
Epithelial cell isolation
Sort Epcam+ cells
Single cell RNA library prep
Sequence
Analysis
b
Distal SI epithelial cells scRNA-seq
Uninfected distal
Infected distal
UMAP 2
UMAP 1
0_Enterocyte
1_Enterocyte
2_Enterocyte
3_Enterocyte
4 _Enterocyte
5_Enterocyte
6_Enterocyte
7_Enterocyte
8_Stem
9_Enterocyte
10_Enterocyte
11_Goblet
12_EEC
13_EEC
14_Enterocyte
c
Pathways enriched by V. cholerae infection
Distal
Enrichment
WP_NUCLEAR_RECEPTORS_METAPATHWAY
REACTOME_SIGNALING_BY_RECEPTOR_TYROSINE_KINASES
REACTOME_RAB_GERANYLGERANYLATION
REACTOME_NEUTROPHIL_DEGRANULATION
REACTOME_INTRA_GOLGI_TRAFFIC
REACTOME_DISEASES_OF_METABOLISM
REACTOME_ASPARAGINE_N_LINKED_GLYCOSYLATION
KEGG_HEMATOPOIETIC_CELL_LINEAGE
HALLMARK_TNFA_SIGNALING_VIA_NFKB
HALLMARK_P53_PATHWAY
HALLMARK_INFLAMMATORY_RESPONSE
HALLMARK_HYPOXIA
qval
d
Pathways enriched by V. cholerae infection
8_Stem
9_Enterocyte
4_Enterocyte
1_Enterocyte
0_Enterocyte
11_Goblet
Qval
Enrichment
Mitosis
Translation, Ribosome
Golgi, ER, mTOR
Metabolism
e
Distal SI
Uninfected
Infected
Percentage
Cluster
f
GO parthway analysis of Cluster 5 enterocytes
antimicrobial humoral response
defense response to bacterium
negative regulation of response to wounding
humoral immune response
regulation of response to wounding
extrinsic apoptotic signaling pathway via death domain receptors
negative regulation of response to external stimulus
regulation of non−canonical NF−kappaB signal transduction
acute inflammatory response
response to wounding
−Log10(p.adjust)
g
Uninfected
Infected
Fgb
Sult6b2
DAPI
100 μm
50 μm
h
Tam at -9h and 0h
Infection
Sampling
-9 h
0 h
20 hpi
Lgr5-Cre+
R26-tdTomato
Tamoxifen
V.c
j
Lgr5-Cre+
R26-tdTomato
0.2 %
tdTom-
tdTom+
% in Sult6b2+ cells
i
Sult6b2
Fgb
tdTomato
DAPI/Fgb/Sult6b2/tdTomato
100 μm
k
Uninfected
Infected
Reg3β
V.c
DAPI
100 μm
l
V.c
20 μm
Reg3β
V.c/Reg3β
m
Pearson's correlation
Reg3β/
V.c

910

Figure 1. *V. cholerae* infection increases the abundance of cluster 5 enterocytes in the small intestine and elicits antimicrobial responses in intestinal epithelial cells in infant mice. **(a)** Experimental scheme of scRNA-seq analysis of epithelial cells. Infant mice (P5) (n=3/group) were infected with *V. cholerae* and sacrificed 20 hours post-infection (hpi). The proximal and distal SI were collected, and epithelial cells were isolated. Single-cell RNA libraries were prepared from sorted Epcam+ cells. **(b)** UMAP of the distal small intestine epithelial single-cell RNA-seq data from uninfected and *V. cholerae* infected P5 infant mice (n=3 for each condition, cells were pooled); EEC, enteroendocrine cells. The arrow indicates cluster 5 enterocytes in infected animals in the distal SI. (**c**) Top-hit pathways from the Single Cell Pathway Analysis (Qval > 8.75 in any cluster). Dot plot represents enrichment in color and Qval in circle size. Stem, stem cells, EC, enterocytes, Gob, Goblet cells, EEC, enteroendocrine cells. (**d**) Volcano plot showing q-value (Qval) and pathway enrichment from Single Cell Pathway Analysis. Pathway enrichment indicates a mean pathway change comparing uninfected and *V. cholerae*-infected conditions. Colors represent the following pathways: Mitosis (green), Translation and Ribosome (light blue), Golgi, ER, and mTOR (pink), and Metabolism (dark blue). (**e**) Percentage of cells in each cluster vs the total cell number in the distal SI. (**f**) GO pathway analysis of cluster 5 representative genes. **(g)** *Fgb* and *Sult6b2* gene detection by single molecule RNA FISH co-stained with DAPI (blue) in the distal SI tissue at 20 hpi. White arrowheads in the higher magnification image indicate the expression of *Fgb* (green) and *Sult6b2* (magenta) mRNA in epithelial cells. Dotted line indicates the epithelial cell membrane. Signal intensity was adjusted to visualize single puncta in the high magnification image. Color-separated images are shown in Extended Data. Fig.3b. (**h**) Experimental protocol for use of lineage tracing to study the origins of cluster 5 cells. To trace the Lgr5 lineage with a pulse of tdTomato labeling, P5 infant mice were treated with 2 doses of tamoxifen (Tam) at -9 and 0 hpi and the small intestine was collected at 20 hpi. (**i**) Representative image of RNA FISH for cluster 5 marker genes *Sult6b2* (red) and *Fgb* (green), protein staining for tdTomato (magenta), and DAPI (blue). White arrowheads show tdTomato+ cells. (**j**) Fraction of tdTomato positive cells (pink) and tdTomato negative cells (white) among *Sult6b2*+ cells. 160 images from 4 animals were analyzed. (**k**) Representative immunostaining of Reg3β (red), *V. cholerae* (magenta), and DAPI (blue) in the distal SI from an uninfected animal (left) or *V. cholerae*-infected animal (right). Scale bar: 100 μm. White arrows show the colocalization of Reg3β and *V. cholerae* on the epithelium. (**l**) Deconvoluted z-stack image of *V. cholerae* (green) and Reg3β (red) from a puncta of Reg3β/*V. cholerae* colocalization image. Overlay image was taken by confocal microscope using x100 lens and z-stack with 0.3 micron gaps per layer. **(m)** Pearson's correlation coefficient between Reg3β and *V. cholerae* co-localization using the images of (**k**) from infected animals. 55 images from 4 animals were analyzed and plotted in a violin plot. (Fig. 1a is partially created in https://BioRender.com.)

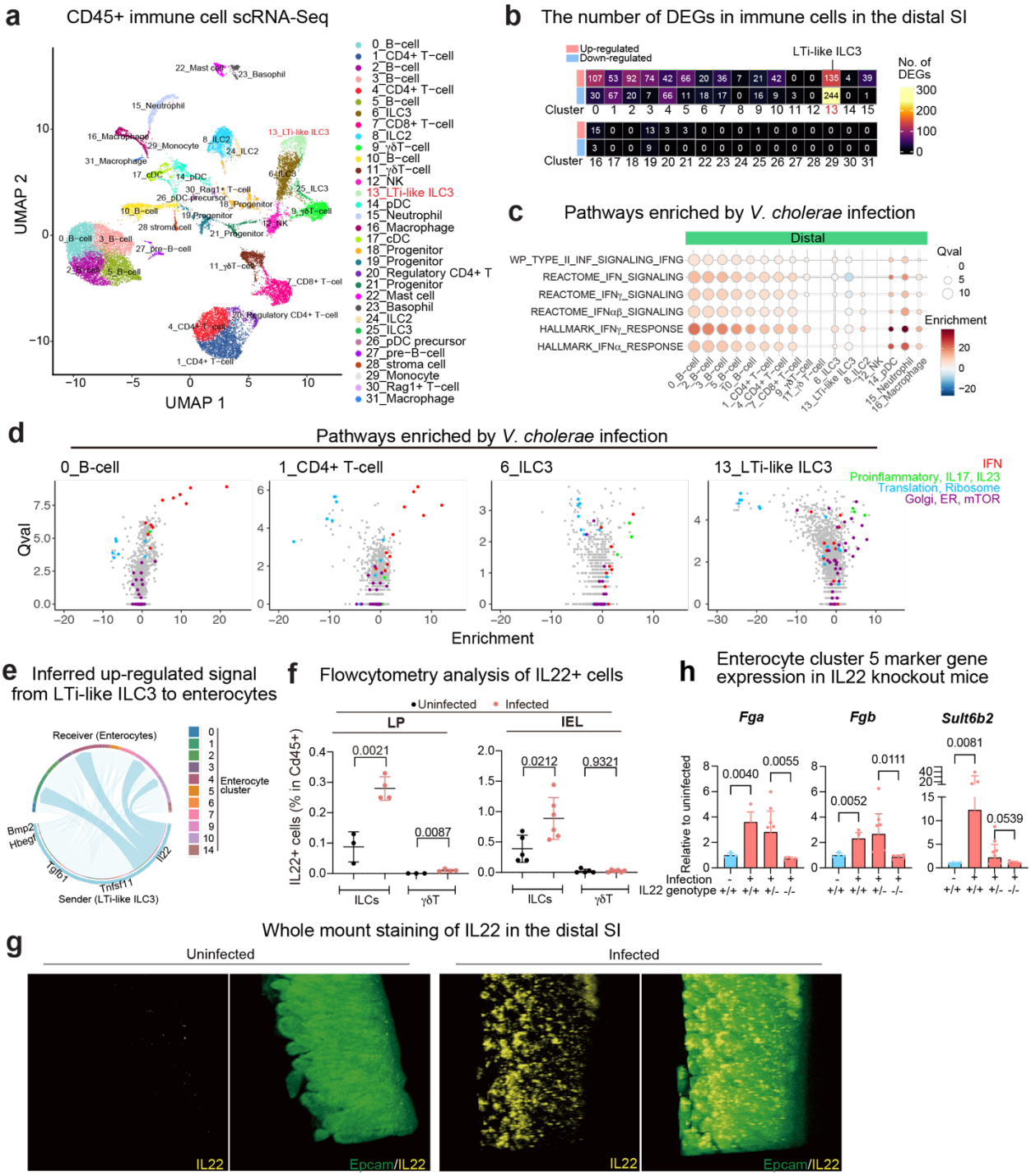

Figure 2. *V. cholerae* infection induces IL22 expression in Type 3 innate lymphoid cells. **(a)** UMAP of CD45+ immune cells (23,836 cells including all conditions: proximal and distal SI, mock and infected samples) in the lamina propria of the small intestine. **(b)** Heatmap of the numbers of differentially expressed genes (absolute Fold Change > 1, adjusted p-value < 0.00001, genes on chromosome X and Y were excluded as both, male and female infant mice were used for each condition, in each cluster). **(c)** Dot plots showing enrichment and Qval of the Single Cell Pathway Analysis results in color and circle size, respectively. Clusters with more than 500 cells (total cell number) isolated from distal SI are shown. **(d)** Volcano plots showing

957 enrichment and Qval of Single Cell Pathway Analysis results in the representative clusters for B
958 cells, T cells, and ILC3s. Colors represent pathways "Interferon" for IFN (red),
959 Proinflammatory, IL17, and IL23 (green), Translation and Ribosome (blue), Golgi, ER, and
960 mTOR (purple). **(e)** CellChat[20]-based analysis of up-regulated signaling pathways from LTi-like
961 ILC3 to enterocytes. IL22-IL22Ra1/IL10Rb signaling is highlighted. Color code represents the
962 types of enterocytes in the receiver. **(f)** IL22+ cell populations in Cd45+ cells in lamina propria
963 (LP, n = 3-4/group) and intraepithelial lymphocyte (IEL, n = 5-6/group). Data are represented as
964 mean ± SD for biological replicates. Unpaired t-test. Data are representative of two independent
965 experiments. **(g)** Whole mount staining of IL22 (yellow) and Epcam (green) in uninfected or
966 infected distal SI. Images are representative of three independent samples/group. (**h**) qPCR
967 analysis of cluster 5 enterocyte marker gene (*Fga*, *Fgb*, and *Sult6b2*) expression in the distal SI
968 from uninfected WT C57BL/6 ($IL22^{+/+}$) (n = 4), *V. cholerae* infected WT C57BL/6 ($IL22^{+/+}$) (n
969 = 5), infected $IL22^{+/-}$ (n = 10) and infected $IL22^{-/-}$ (n = 5) littermate animals. Expression levels
970 were normalized to β-Actin expression and shown as relative expression to uninfected $IL22^{+/+}$
971 group. Data are represented as mean ± SD. Brown-Forsythe and Welch ANOVA.

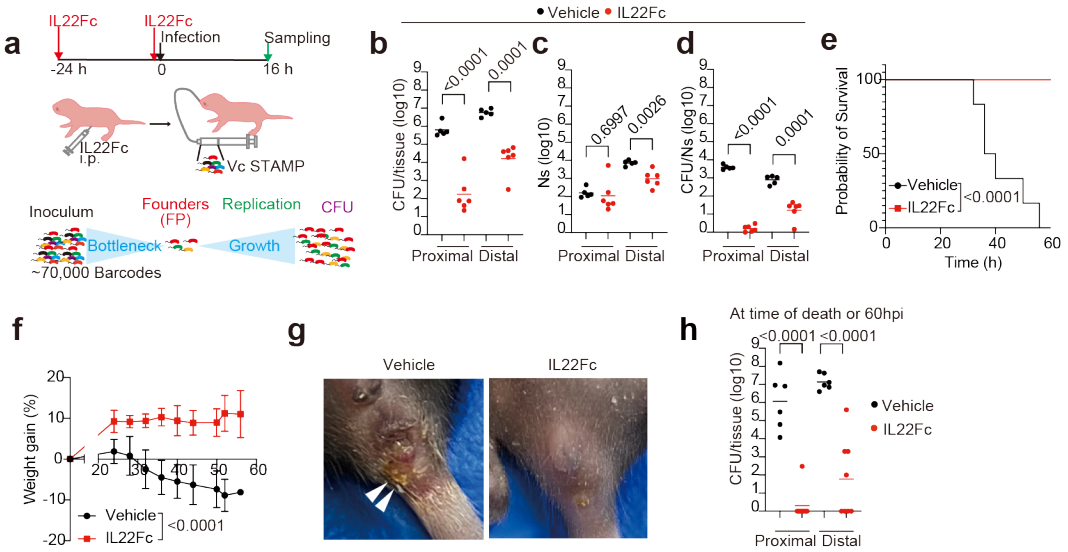

Figure 3. IL22 treatment protects infant mice from experimental cholera.
(a) Schematic of IL22 prophylactic regime. A barcoded library of *V. cholerae* was used in these experiments to enable measurement of the founding population (Ns), the number of cells from the inoculum that establish infection, and CFU/Ns which represents the net replication of the founders during infection. **(b-d)** CFU (b), founding population (Ns) (c), and replication (CFU/Ns) (d) of *V. cholerae* in the proximal and distal SI. Vehicle: PBS-treated animals, IL22Fc: IL22Fc-treated animals. Bars indicate the geometric mean for biological replicates (n = 5-6/group). Unpaired t-test. **(e)** Kaplan-Meyer plot of infant mice survival in *V. cholerae* infection in IL22Fc-treated or control animals; vehicle control (black, n = 6), IL22Fc-treated group (red, n = 8). Log-rank test. **(f)** Percent weight gain relative to the time of infection; vehicle (black, n = 6), IL22Fc-treated group (red, n = 8). Data are represented as mean ± SD. Two-way ANOVA. **(g)** Diarrhea in *V. cholerae*-infected infant mice at 48 hpi. White arrowheads in vehicle-treated animals point to clear diarrheal fluid on the anus. **(h)** *V. cholerae* burden in the proximal and distal SI at the time of death (vehicle-treated, black, n = 6) or 60 hpi (IL22Fc-treated, red, n = 8). Bars indicate the geometric mean. Unpaired t-test. P-values are shown.

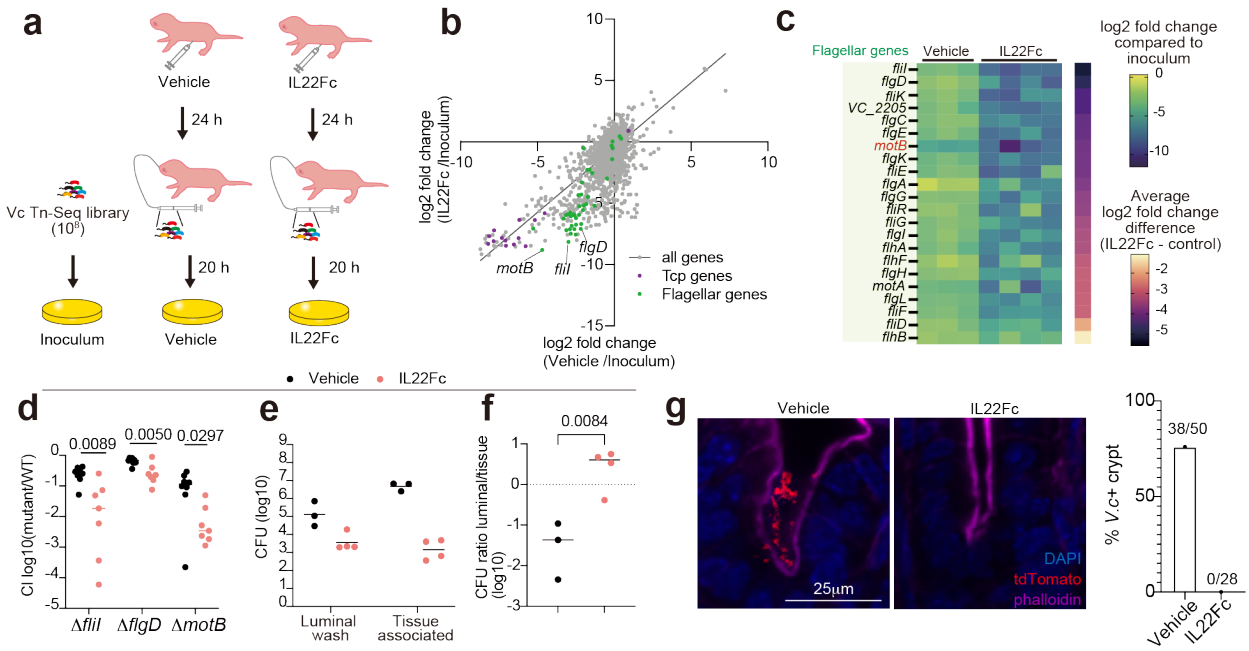

Figure 4. IL22Fc treatment modifies *V. cholerae* colonization requirements

(a) Experimental scheme of the transposon-insertion sequencing screen. Mice were given vehicle (PBS, n = 3) or 5µg of IL22Fc (n = 4) at 24 hours before infection and were infected with 10^8 cells of a *V. cholerae* transposon library. SI tissues were harvested at 20 hpi. **(b)** XY plot of transposon insertion frequency compared to inoculum (culture on LB plates); x-axis represents the mean of $\log_2$ fold change (bacteria recovered from distal SI of PBS-treated mice vs. inoculum) and y-axis represents the mean of $\log_2$ fold change (bacteria recovered from distal SI of IL22Fc-treated mice vs. inoculum). Purple dots: Tcp-biogenesis mutants; green dots: Flagellar-related mutants. The plot represents the mean value of biological replicates (Control: n = 3, IL22Fc: n = 4). **(c)** Heatmap representing $\log_2$ fold change of transposon insertion frequency in flagellar genes in samples recovered from mouse tissue compared to inoculum. Column and row show individual mouse and *V. cholerae* genes, respectively. The magma color heatmap indicates the difference in the average of $\log_2$ fold change between IL22Fc-treated mice vs. control mice. **(d)** Competitive index (CI) using barcoded mutant vs. WT strains in vehicle (black, n = 8) and IL22Fc-treated animals (red, n = 7). Multiple unpaired t-tests were performed between control vs IL22Fc-treated animals. Bars indicate the geometric mean. **(e)** CFU of *V. cholerae* detected in the luminal wash and attached to the tissue of the distal SI in vehicle-treated animals (black, n = 3) and IL22Fc-treated animals (red, n = 4). **(f)** Ratio of bacterial CFU in luminal washes compared with CFU of tissue-associated bacteria in vehicle-treated (black, n = 3) or IL22Fc-treated animals (red, n = 4). Unpaired t-test. **(g)** Representative images of WT *V. cholerae* colonization in the crypt in control animal (left image) and IL22Fc-treated animal (right image), and a bar graph showing the percent of crypts occupied by *V. cholerae* in the distal SI. Blue: DAPI, red: *V. cholerae LacZ::tdTomato*, magenta: phalloidin for actin staining. Scale bar: 25 µm. P-values are shown in individual figures.

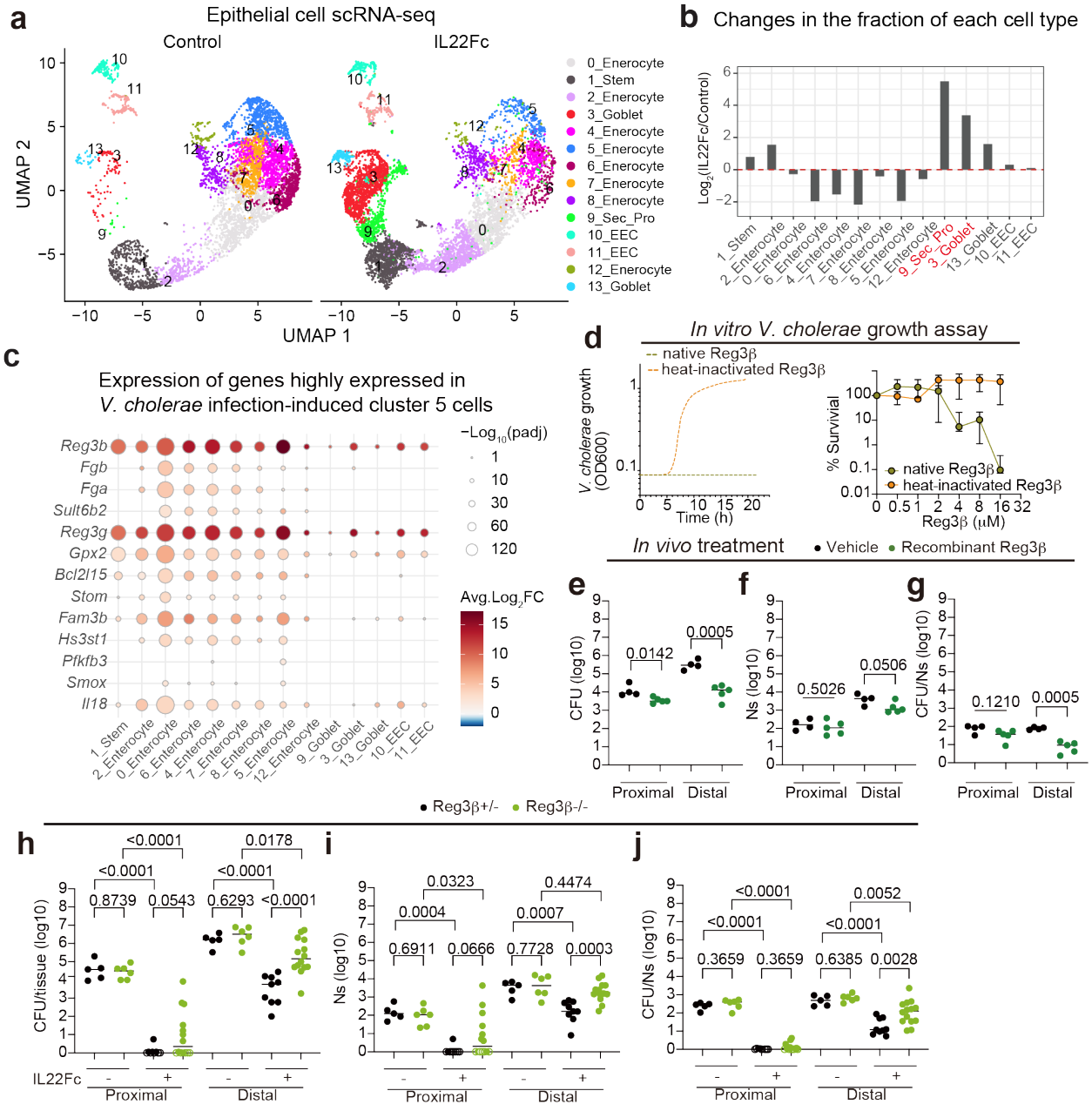

Figure 5. IL22Fc treatment alters intestinal epithelial cell transcriptional profiles. **(a)** UMAP of epithelial single-cell RNA-seq data of the distal small intestine in P5 infant mice in control and IL22Fc-treated animals. **(b)** Comparison of cluster abundance between IL22Fc-treated and untreated control animals. **(c)** Dot plot representing control vs. IL22Fc-treated gene expression changes of cluster 5 cell marker genes (Fig. S3a) in epithelial cell subsets. Color represents average $\log_2$ fold change of gene expression compared to untreated control. Dot size represents negative $\log_{10}$-scaled adjusted p-value. **(d)** *V. cholerae* growth curve measured by OD600 after incubation with native or heat-inactivated Reg3β (left). Percent *V. cholerae* survival after incubation with indicated concentration of Reg3β (right). Data represent mean ± SD for experimental replicates; native Reg3β (n = 4/condition), heat-inactivated Reg3β (n = 2/condition). **(e-g)** CFU (e), founding population (Ns) (f), and CFU/Ns (g) of *V. cholerae* in the

1025 proximal and distal SI at 16 hpi. Infant mice were orally administered 2 doses of vehicle (PBS, n
1026 = 4) or Reg3β recombinant protein (33 μg/dose, n = 5) at -0.5 and +1 hpi. Bars represent the
1027 geometric mean for biological replicates. One-way ANOVA. (**h-j)** CFU (h), Ns (i), and CFU/Ns
1028 (j) of *V. cholerae* in the proximal and distal SI of P5 Reg3β-/- mice and heterozygous littermate
1029 at 16 hpi. Bars represent the geometric mean for biological replicates. Open circles indicate no
1030 CFU detected. One-way ANOVA. Sample groups were compared among the same tissue. P-
1031 values are shown.

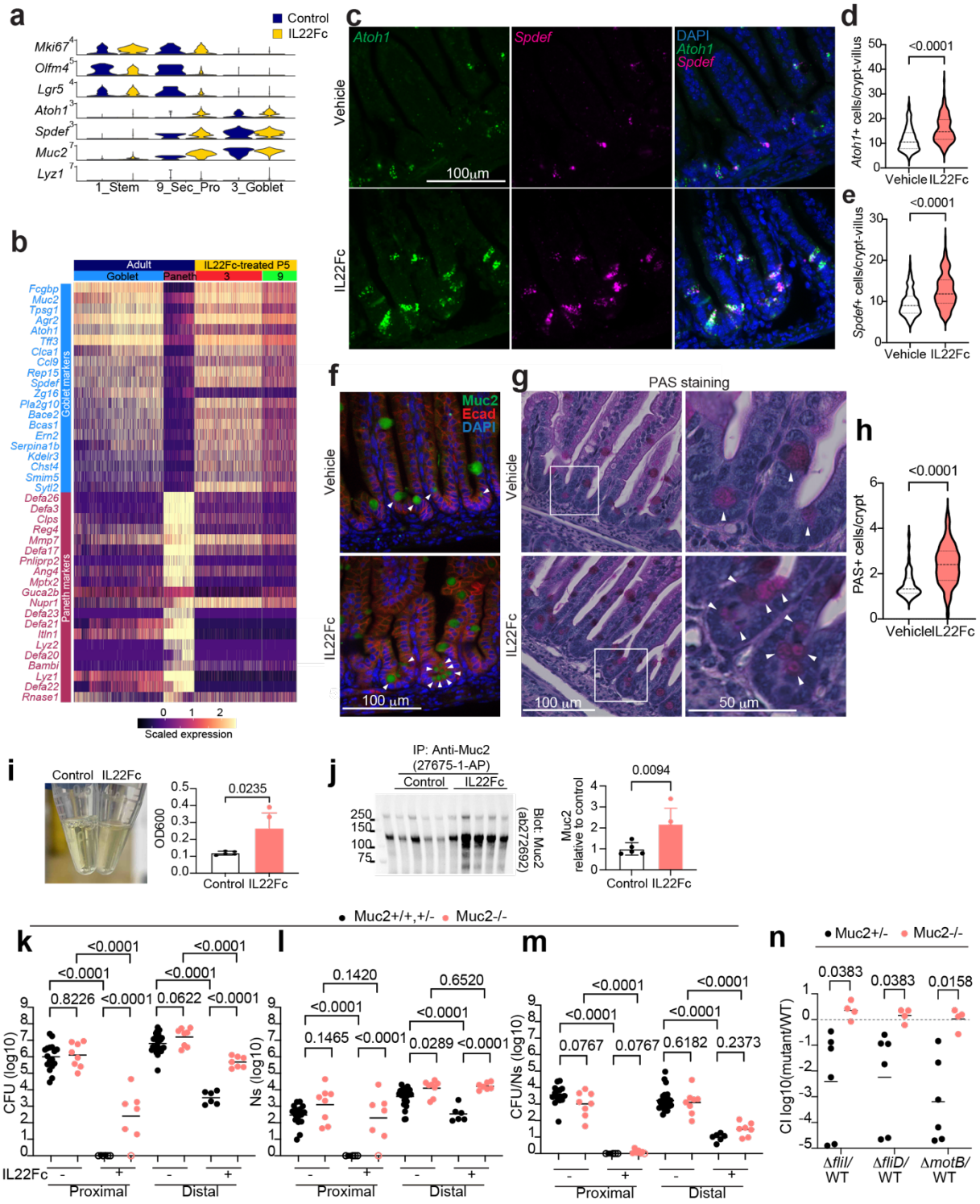

Figure 6. IL22Fc expands Goblet cells and Muc2 production is critical for IL22-mediated protection against *V. cholerae* colonization.

(a) Violin plot of traditional marker gene expression in stem cells, secretory progenitor cells, and goblet cells. *Lgr5* and *Olfm4*: stem cell marker, *Mki67*; proliferating cell marker, *Atoh1* and *Spdef*; secretory progenitor cell marker, *Muc2*: Goblet cell marker, *Lyz1*: Paneth cell marker. **(b)** Heatmap of goblet and Paneth cell marker expression in adult (Haber et al: GSE92332[73]) and

1039 IL22Fc-treated P5 infant mice. (**c)** Representative RNAScope images of *Atoh1* (green) and *Spdef*
1040 (magenta) expression in the epithelial cells in the crypts of the distal small intestine of vehicle-
1041 and IL22Fc-treated infant mice. (**d, e)** The number of *Atoh1*+ (d), or *Spdef*+ (e) cells in the SI
1042 epithelium. Vehicle: n = 122 images from 4 animals, IL22Fc: n = 141 images from 4 animals.
1043 Unpaired t-test. (**f)** Representative images of immunohistochemistry of E-Cadherin (red), Muc2
1044 (green), and DAPI (blue) in the distal small intestine of vehicle- and IL22Fc-treated animals.
1045 White arrowheads point to the Muc2+ cells in the crypts. (**g)** PAS staining of the distal small
1046 intestine of vehicle and IL22Fc treated animals. Arrowheads indicate PAS+ cells in the crypt.
1047 Vehicle: n = 63 images from 3 animals, IL22Fc: n = 65 images from 3 animals. (**h)** Enumeration
1048 of PAS+ cells in the crypts. Unpaired t-test with Welch's correction. (**i**) Western blot image of SI
1049 luminal wash detected with anti-Muc2 antibody. n = 5/group. **(i)** Appearance of luminal washes
1050 collected from control and IL22Fc-treated infant mice (left). Turbidity of luminal washes were
1051 measured as OD600 in a spectrophotometer (right). **(j)** Immunoprecipitation-western blot for
1052 Muc2 in luminal washes (right blot) and the signal intensity analyzed by densitometry (right bar
1053 graph). Signal intensity was normalized by the average intensity in control samples. n =5/group.
1054 (**k-m)** CFU (k), FP (l), and replication (CFU/FP) (m) of *V. cholerae* in the small intestine of P5
1055 infant $Muc2^{-/-}$ vs littermate wild type or heterozygous controls ($Muc2^{+/+, +/-}$) animals treated with
1056 (+) or without (-) IL22Fc. n = 6-28 animals/group. Bars represent the geometric mean for
1057 biological replicates. One-way ANOVA. Sample groups were compared among the same tissue.
1058 P-values are indicated in individual plots. Open circles indicate no CFU detected. (**n**)
1059 Competitive index (CI) using barcoded mutant vs. WT *V. cholerae* strain in infant $Muc2^{-/-}$ (n = 4,
1060 pink) or heterozygous littermate control (n = 6, $Muc2^{+/-}$, black) mice treated with a single dose of
1061 5 μg of IL22Fc 24 hours before infection. Bars represent the geometric mean for biological
1062 replicates. Multiple t-test with fold discovery rate. Corrected q-values are indicated in individual
1063 comparison.

Extended Data Figures

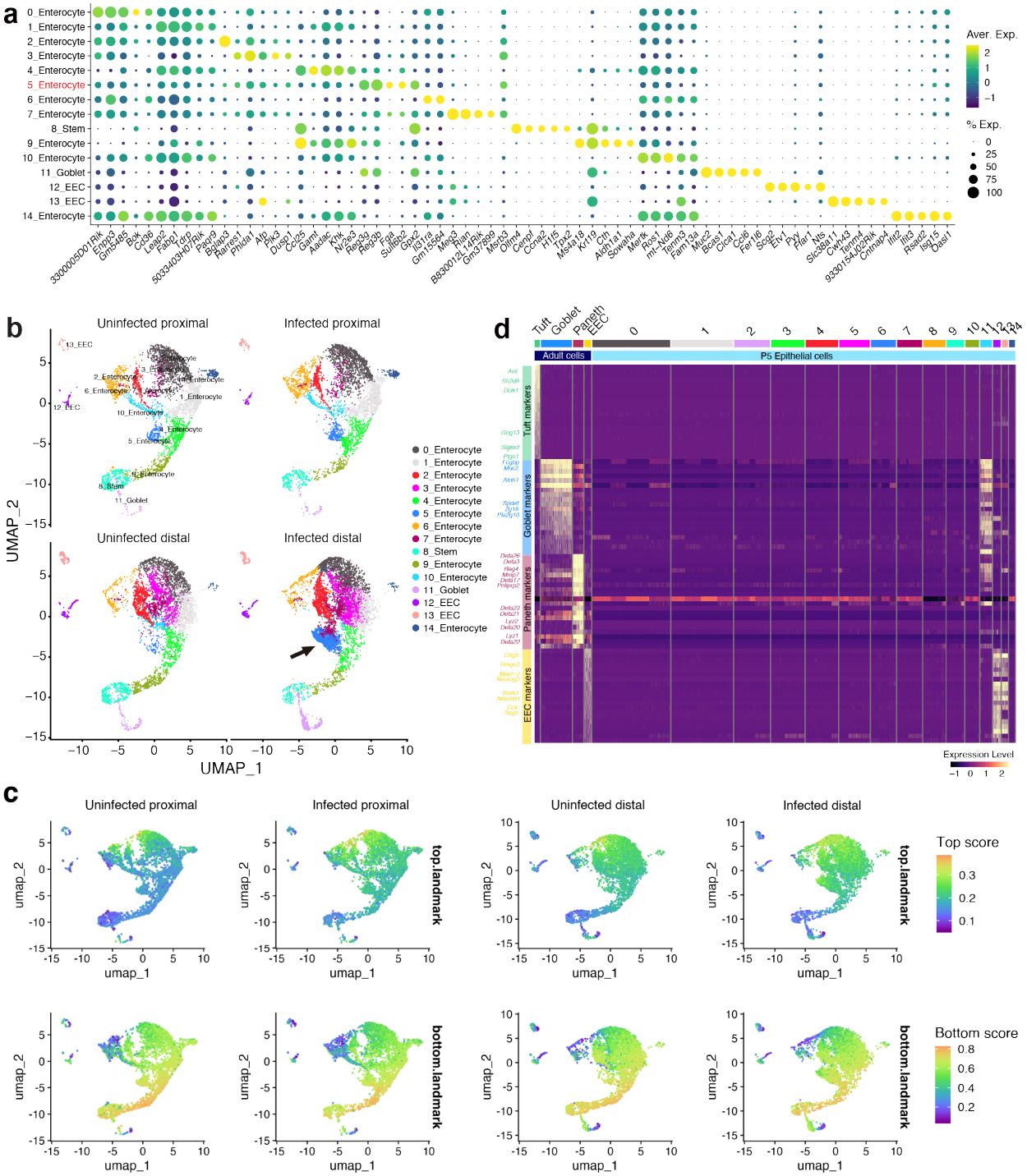

Extended Data Fig. 1. scRNA-seq profile of the SI epithelial cells in P5 infant

(a) Representative genes for each epithelial cell cluster depicted in Fig.1b. Dot plot indicates the scaled expression levels in color and the percentage of the cells expressing genes in the size of each cluster; EEC, enteroendocrine cells. **(b)** UMAP of the small intestinal epithelial single-cell RNA-seq data of the proximal and distal SI from uninfected and *V. cholerae* infected P5 infant mice (n=3 for each condition, cells are pooled). The arrow points cluster 5 enterocytes in

1072 infected animals in the distal SI. **(c)** Signature scores of top-villus landmark genes (left panels)
1073 and bottom-villus landmark genes (right panels) calculated by UCell[74] . Color scales indicate the
1074 UCell score. (**d)** Marker genes for tuft cell (green), goblet cell (blue), Paneth cell (red) and
1075 enteroendocrine cell (EEC, yellow) and their expression in epithelial cell clusters in adult (Haber
1076 et al[73] : GSE92332) and P5 infant mice. Heatmap represents the scaled expression level.

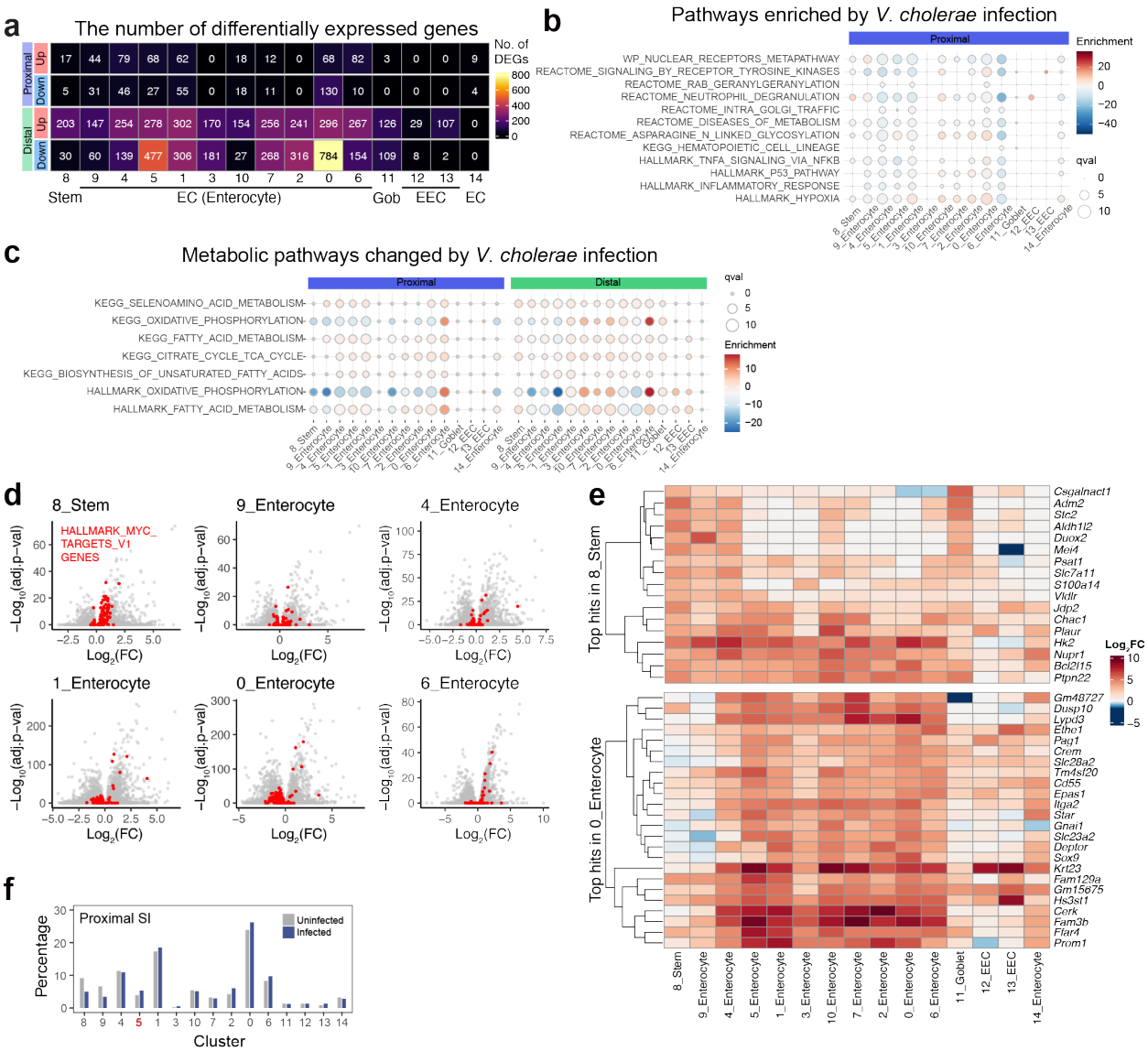

Extended Data Fig. 2 Epithelial cell-type specific responses to *V. cholerae* infection
(a) Heatmap of the numbers of differentially expressed genes (absolute Fold Change > 1, adjusted p-value < 0.00001, genes on chromosome X and Y were excluded as both, male and female infant mice were used for each condition) in each cluster. Stem, stem cells, EC, enterocytes, Gob, goblet cells, EEC, enteroendocrine cells. (**b**) Pathways of the Single Cell Pathway Analysis (Qval > 8.75 in any cluster) in the proximal SI epithelium. Pathways are matched to Fig.1c. Dot plot represents enrichment in color and Qval in circle size. Stem: stem cells; Gob: Goblet cells; EEC: enteroendocrine cells. **(c)** HALLMARK and KEGG metabolic pathways altered by *V. cholerae* infection. Dot plot represents enrichment in color and Qval in circle size. **(d)** Volcano plots showing gene expression changes between uninfected and *V. cholerae*-infected conditions. Genes in the HALLMARK_MYC_TARGETS_V1 pathway are highlighted as red. **(e)** Heatmap representing uninfected vs. *V. cholerae*-infected gene expression changes in color. Top: Top-hit DEGs (Log_2 fold change > 3 and adjusted p-value < 0.01) in 8_stem, Bottom: Top-hit DEGs in 0_Enterocyte. *Reg3b* and *Reg3g* are excluded. Note that log_2 fold change of the genes without any values of differential expression analysis (Seurat's

1093 FindMarkers function) are set to zero. (**f**) Percentage of cells in each cluster vs the total cell
1094 number in the proximal SI.

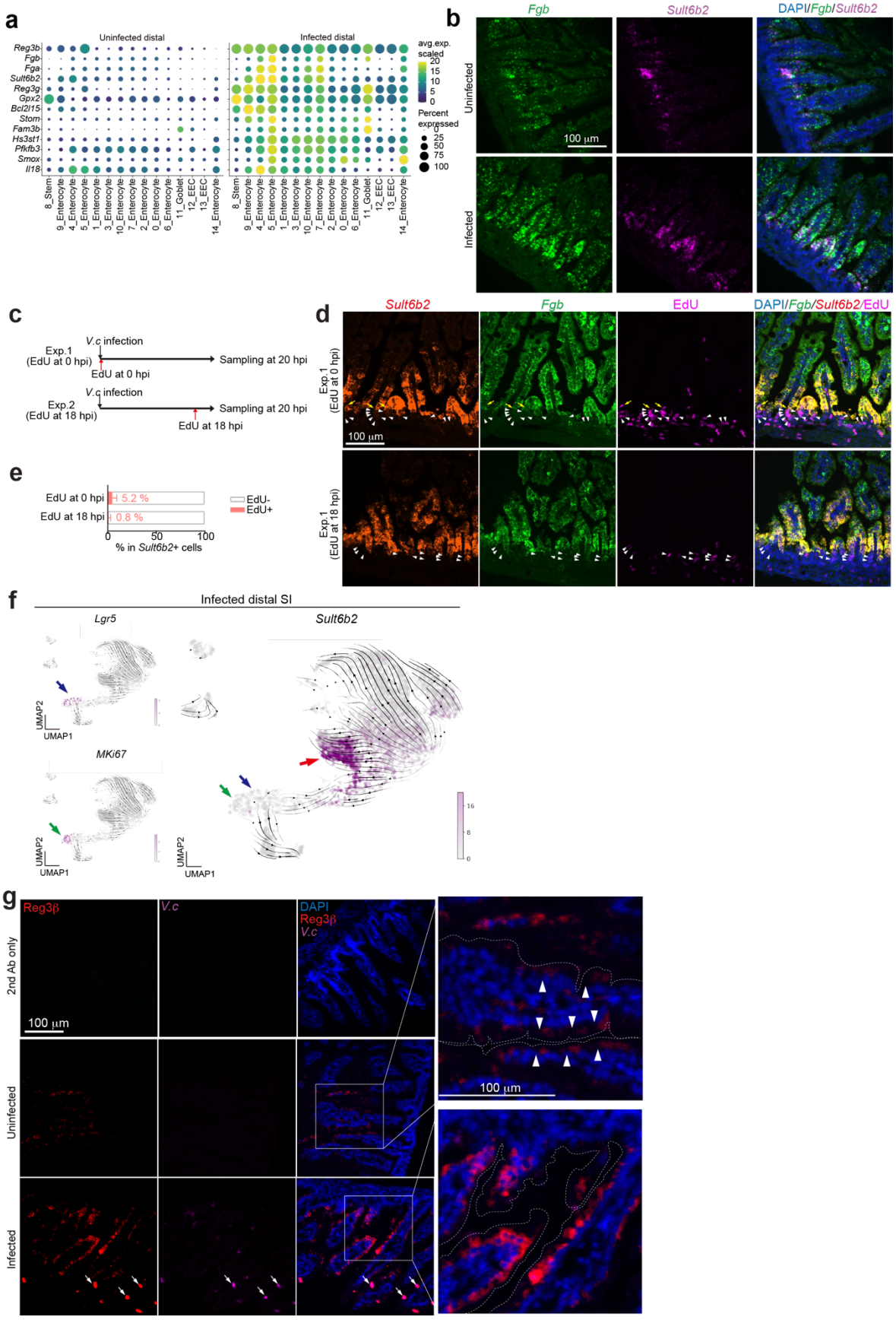
a
Uninfected distal
Infected distal
Reg3b
Fgb
Fga
Sult6b2
Reg3g
Gpx2
Bcl2l15
Stom
Fam3b
Hs3st1
Pfkfb3
Smox
Il18
8_Stem
9_Enterocyte
4_Enterocyte
5_Enterocyte
1_Enterocyte
3_Enterocyte
10_Enterocyte
7_Enterocyte
2_Enterocyte
0_Enterocyte
6_Enterocyte
11_Goblet
12_EEC
13_EEC
14_Enterocyte
avg.exp. scaled
Percent expressed
b
Fgb
Sult6b2
DAPI/Fgb/Sult6b2
Uninfected
Infected
100 μm
c
Exp.1 (EdU at 0 hpi)
V.c infection
Sampling at 20 hpi
EdU at 0 hpi
Exp.2 (EdU at 18 hpi)
EdU at 18 hpi
d
Sult6b2
Fgb
EdU
DAPI/Fgb/Sult6b2/EdU
Exp.1 (EdU at 0 hpi)
Exp.1 (EdU at 18 hpi)
100 μm
e
EdU at 0 hpi
5.2 %
EdU at 18 hpi
0.8 %
EdU-
EdU+
% in Sult6b2+ cells
f
Infected distal SI
Lgr5
Sult6b2
MKi67
UMAP1
UMAP2
g
Reg3β
V.c
DAPI
2nd Ab only
Uninfected
Infected
100 μm

1095

1096 **Extended Data Fig. 3. Identity of cluster 5 epithelial cells**
1097 **(a)** Representative genes for cluster 5 epithelial cells. Dot plots indicate the scaled expression
1098 levels in color and the percentage of the cells expressing genes in the size of each cluster of
1099 epithelial cells in distal SI in uninfected (left panel) and *V. cholerae* infected animals (right
1100 panel).(**b**) Separated images of RNA FISH detecting cluster 5 markers: *Fgb* (green) and *Sult6b2*
1101 (magenta). DAPI (blue). Merged images are also shown in Fig. 1g. (**c**) Experimental protocols
1102 for experiments with EdU labeling and imaging to investigate the origins of cluster 5 cells. In
1103 experiment 1 (Exp. 1), infant mice were given EdU at the same time of infection (0 hpi), and in
1104 experiment 2 (Exp 2), infant mice were given EdU at 18 hpi (2 hours before sampling). (**d**)
1105 Representative images of EdU (magenta), co-stained with cluster 5 enterocyte markers, *Sult6b2*
1106 (red) and *Fgb* (green), and DAPI. (**e**) The percentage of EdU+ cells in cluster 5 enterocytes
1107 (*Sult6b2*+ cells). 110 (from 4 mice, Exp.1) and 63 images (from 3 mice, Exp.2) were analyzed.
1108 (**f**) UMAP projection representing the RNA expression of marker genes in the epithelial cell
1109 scRNA-seq data from the distal SI in infected animals. RNA-velocity is overlayed on the UMAP.
1110 Top left UMAP shows the expression levels of *Lgr5* (stem cells) and the bottom left UMAP
1111 shows that of *MKi67* in purple. The right UMAP shows the expression level of cluster 5
1112 enterocyte marker gene *Sult6b2* in purple. Colored arrows on the UMAPs point to *Lgr5*+ cells
1113 (blue), *MKi67*+ cells (green), and *Sult6b2*+ cells (red). (**g**) Immunohistochemistry of Reg3β
1114 (red), *V. cholerae* (magenta), and DAPI (blue) in the distal SI tissue at 20 hpi. Top row images
1115 depict tissues stained with only secondary antibody as a control. Middle and bottom rows are
1116 uninfected and *V. cholerae* infected distal SI tissues. White arrows in the images of infected
1117 samples show *V. cholerae* microcolonies on the SI villi. Right panels are high magnification
1118 images of the merged image. White arrowheads in the high magnification image indicate the
1119 expression of Reg3β in the uninfected SI. Dotted line indicates the epithelial cell membrane.
1120 Merged images are also shown in Fig. 1k. Scales are indicated.

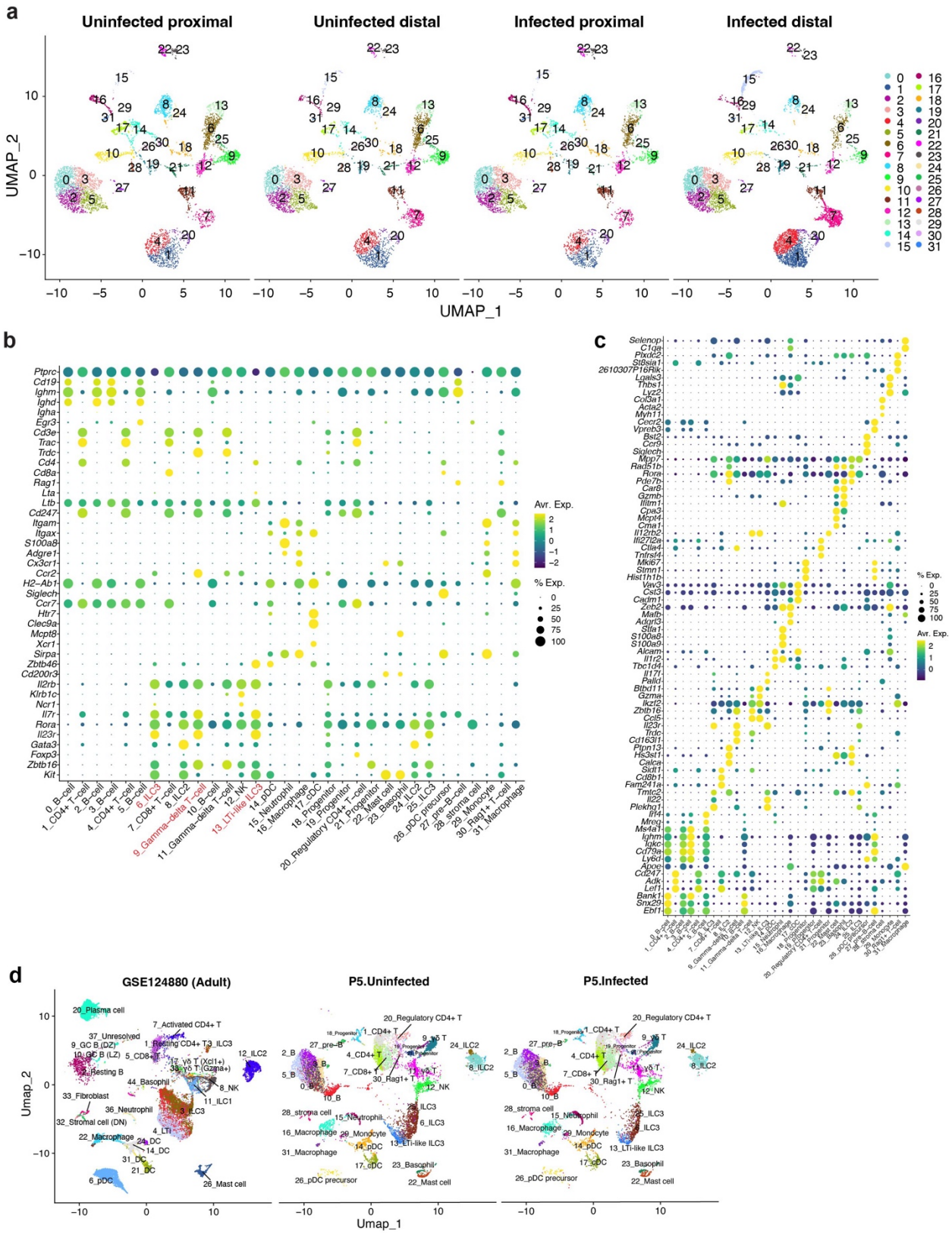

Extended Data Fig. 4. scRNA-seq profile of the SI lamina propria CD45+ cells in P5 infant mice.

1124 **(a**) UMAP of the CD45+ cells, split by tissue (proximal and distal) and conditions (infected and
1125 uninfected). **(b, c)** Canonical marker gene (b) and representative gene expression (c) in each
1126 cluster. Canonical marker genes were determined by database search with Tabula Muris[75],
1127 PanglaoDB[76] , and literatures[77–79]. Dot plot indicates the scaled expression levels in color and the
1128 percentage of the cells expressing genes in the size of each cluster of immune cells in combined
1129 data (immune cells in proximal and distal SI from uninfected and infected animals).
1130 **(d**) Integrated UMAP of the immune cells in adult (GSE124880)[18] and infant mice (our data).
1131 GSE124880 cell annotations are based on the original data source.

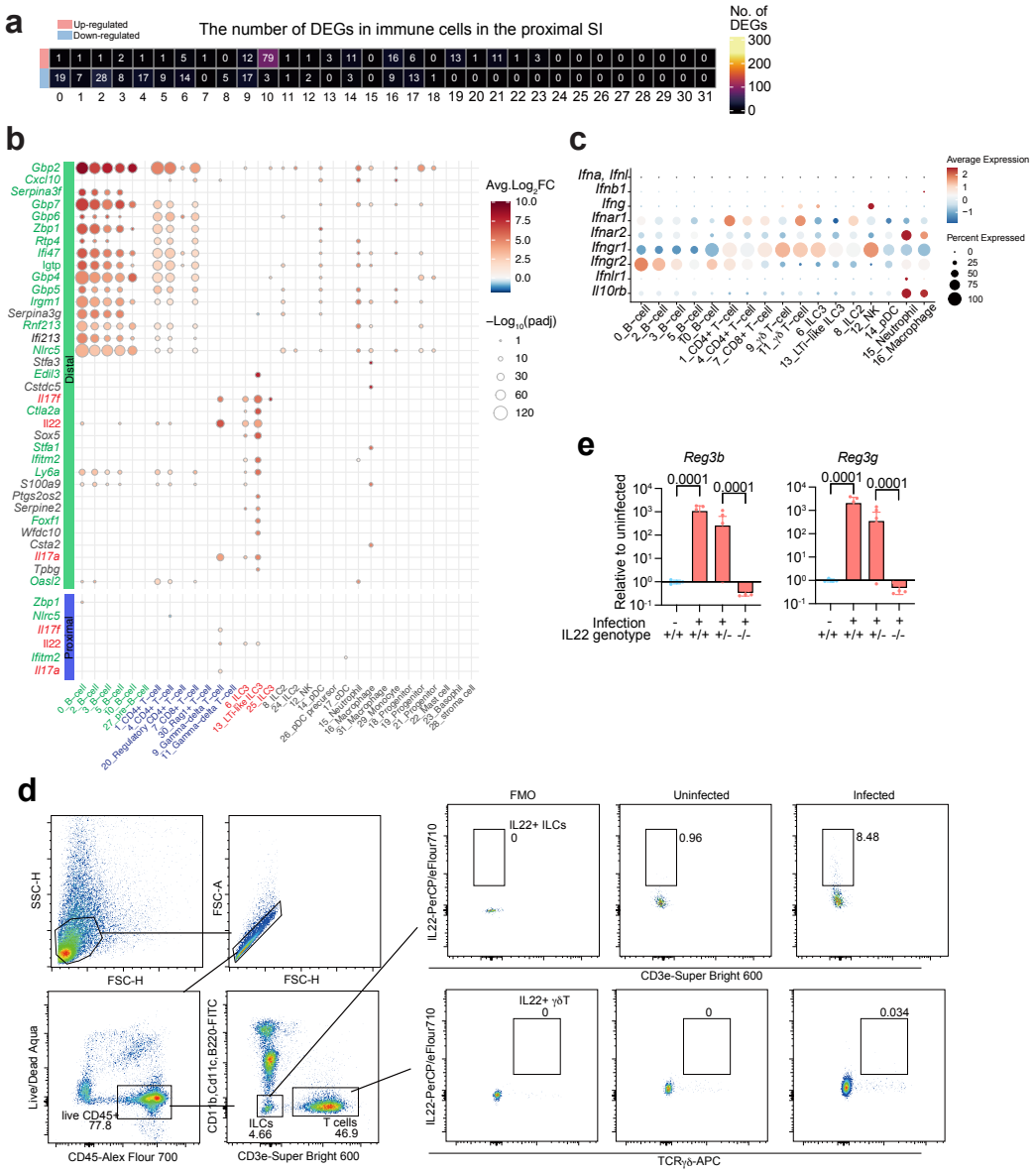

Extended Data Fig. 5 Cell-type specific transcriptional change

(a) Heatmap of the numbers of differentially expressed genes (absolute Fold Change > 1, adjusted p-value < 0.00001, genes on chromosome X and Y were excluded as both, male and female infant mice were used for each condition, in each cluster). (**b**) Top upregulated genes in the distal small intestine (Fold Change > 3, adjusted p-value < 10^{-20}, on Autosomes, at least 20% of the cells in cluster express the gene). The expression of the several top-upregulated genes in the distal SI also changes in the proximal SI. *Il22*, *Il17a*, and *Il17f* are highlighted in red. Interferon responsive genes are highlighted in green. Color shows the average $\log_2$ fold change. Dot size represents negative $\log_{10}$ scaled value of adjusted p-value. **(c)** Dot plots showing average expression and percent of expressing cells of interferons and their receptor gene expression in immune cells. Clusters with more than 500 cells (total cell number) are shown. Note that *Ifna* and *Ifnl* were not detected. Color shows the average expression. Dot size

1145 represents percent of cells expressing genes in each cluster. **(d)** Representative flow cytometry
1146 plots for IL22+ ILCs (CD45+, CD11b-, CD11c-, B220-, CD3e-, IL22+) and γδT cells (CD45+,
1147 CD11b-, CD11c-, B220-, CD3e+, TCRγδ+, IL22+) detection in SI lamina propria. FMO:
1148 Fluorescence minus one (anti-Il22 antibody) control. **(e)** qPCR analysis of *Reg3b* and *Reg3g*
1149 expression in the distal SI from *V. cholerae* infected/uninfected WT C57BL/6 ($IL22^{+/+}$), infected
1150 $IL22^{+/-}$ and $IL22^{-/-}$ littermate animals. Expression levels were normalized by β-Actin expression
1151 and shown as relative expression to uninfected $IL22^{+/+}$ group.

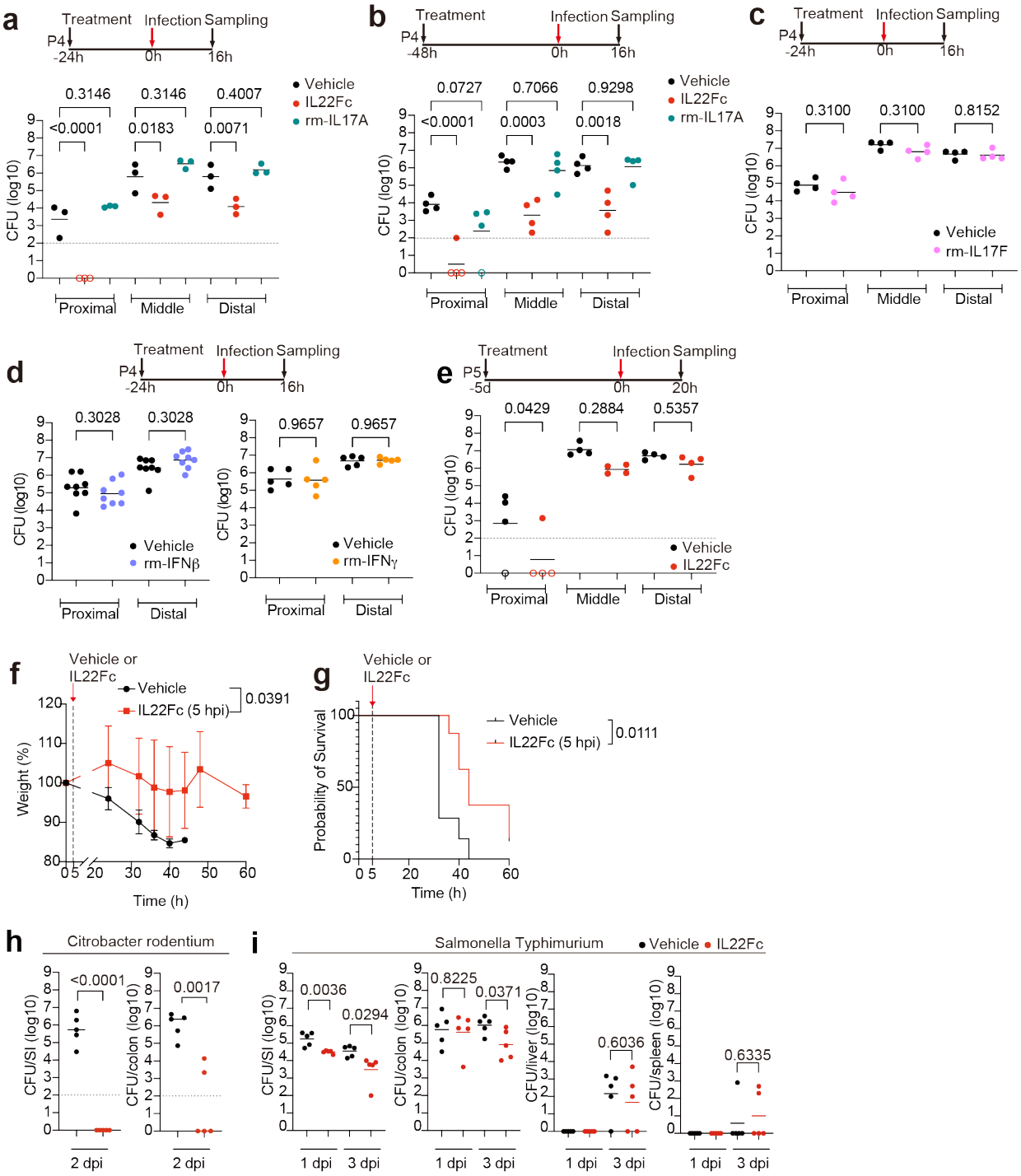

Extended Data Fig. 6. Dosage regimen-dependent efficacy of IL22Fc on *V. cholerae* colonization and effect of IL22Fc on colonization with other enteric pathogens

(a, b) *V. cholerae* burden in the SI tissues in animals treated with vehicle (black), 5μg IL22Fc (red), or 5 μg mouse recombinant IL17A (rm-IL17A) (green) 24 h (a) or 48 h (b) before infection. **(c, d)** *V. cholerae* burden in the SI tissues in animals treated with vehicle (black) or 5μg mouse recombinant IL17F (rm-IL17F) (pink) (c), 5000 unit of recombinant mouse IFNβ (rm-IFNβ, purple) or 2 μg of recombinant mouse IFNγ (rm-IFNγ, orange) (d) 24 h before

1160 infection. **(e)** *V. cholerae* burden in the SI tissues in animals treated with vehicle (black) or 5µg
1161 IL22Fc (red) 5 days before infection. One-way ANOVA. **(f, g)** Percent of body weight compared
1162 to that at 0 hpi (f) and survival (g) after *V. cholerae* infection. Mice were infected with WT *V.*
1163 *cholerae* and administered vehicle or IL22Fc i.p. at 5 hpi. Data are represented as mean ± SD for
1164 biological replicate (n = 7-8/group), Two-way ANOVA (f). Log-rank test (g). **(h)** *C. rodentium*
1165 burden in the entire SI and colon in vehicle (black) or IL22Fc-treated (red) infant animals at 2-
1166 days post infection (dpi). Bars indicate the geometric mean for biological replicates (n =
1167 5/group), Unpaired t-test. The dotted lines indicate the detection limit. (**i)** *S.* Typhimurium
1168 burden in the entire SI, colon, liver, and spleen in vehicle (black) or IL22Fc-treated (red) infant
1169 animals at 1- or 3 dpi. One-way ANOVA. (a, b, c, d, g, h) Bars indicate the geometric mean for
1170 biological replicates. P-values are shown.

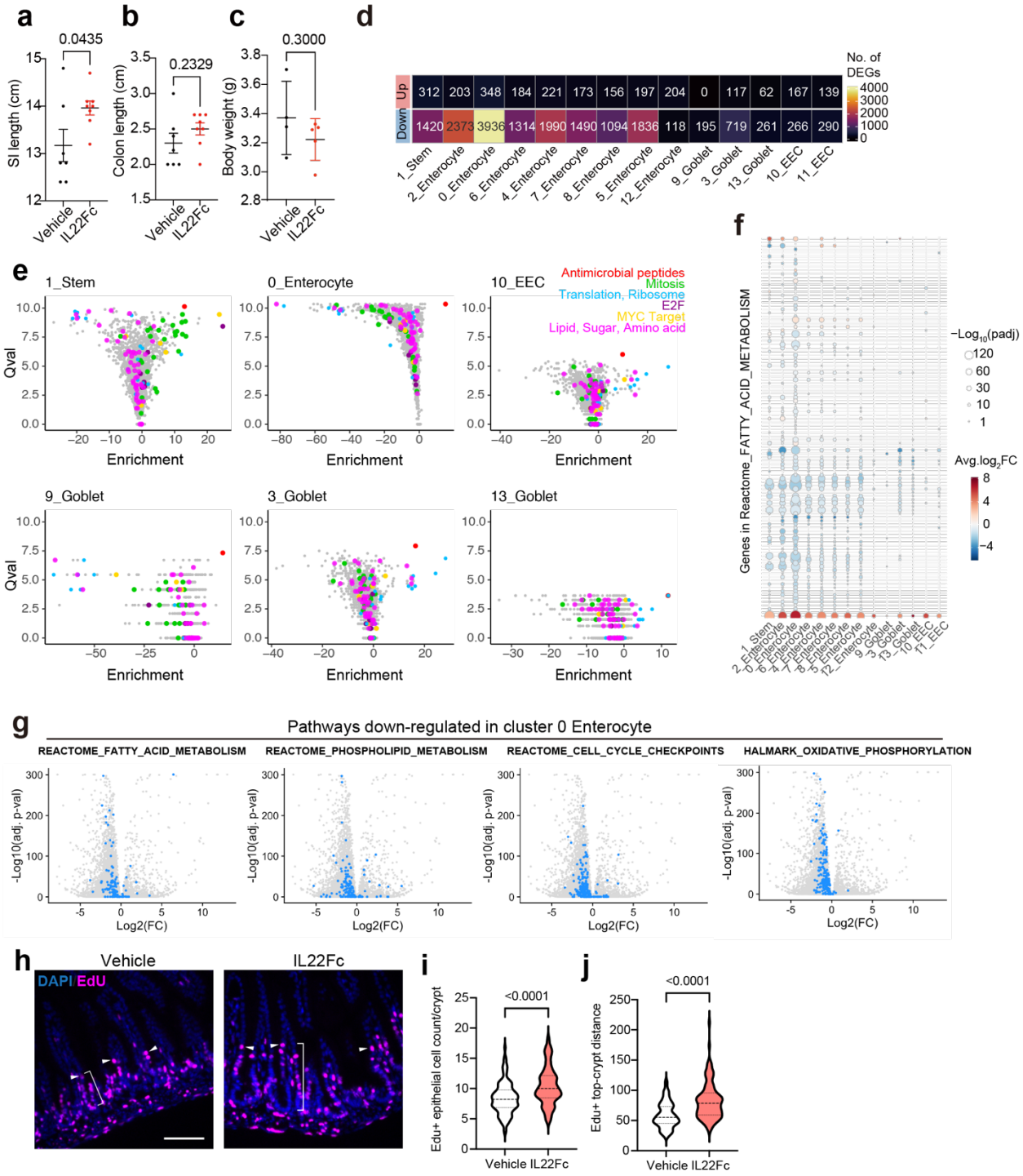

Extended Data Fig. 7. IL22Fc administration alters the SI epithelium

(**a-c**) SI (a) and colon (b) length, and body weight (c) of animals 40 hours after vehicle (black) or IL22Fc (red) administration. Data are represented as mean ± SD for biological replicate (n = 7-8/group for the measurement of SI and colon length, n = 4-5/group for the measurement of body weight). Unpaired t-test. P-value is indicated in individual plots. (**d**) Heatmap of the numbers of differentially expressed genes (absolute Fold Change > 1, adjusted p-value < 0.00001, genes on chrX and Y were excluded as male and female infants were mixed) in each cluster. (**e**) Volcano

1179 plots showing fold change and q-value of Single Cell Pathway Analysis results. Colors represent
1180 pathways: Antimicrobial peptides (red), Mitosis (yellow green), Translation and Ribosome (light
1181 blue), E2F (purple), MYC Target (yellow), and Lipid, Sugar, Amino acid (pink). (**f**) Dot plot
1182 represents control vs. IL22Fc-treated gene expression changes in the
1183 REACTOME_FATTY_ACID_METABOLISM pathway. Average of $\log_2$ fold change in
1184 IL22Fc-treated compared to control is shown in color and negative $\log_{10}$-scaled adjusted p-value
1185 is shown in the size of each cluster. (**g**) Volcano plots show differentially expressed genes
1186 between IL22Fc- vs. control-treated animals in cluster 0 enterocytes. The x- and y-axis indicate
1187 $\log_2$ fold change compared to control animals and negative $\log_{10}$ adjusted p-value, respectively.
1188 Genes in REACTOME_FATTY_ACID_METABOLISM,
1189 REACTOME_PHOSPHOLIPID_METABOLISM,
1190 REACTOME_CELL_CYCLE_CHECKPOINTS, and
1191 HALLMARK_OXIDATIVE_PHOSPHORYLATION pathways are highlighted in blue.
1192 (**h**) Representative images of 5-ethynyl 2′-deoxyuridine (EdU) positive cells in the distal small
1193 intestine. P4 infant mice were intraperitoneally treated with vehicle or IL22Fc, and EdU. Mice
1194 were sacrificed at 36 h post administration. DNA-incorporated EdU was stained with Alexa 647
1195 (magenta). White arrowheads point to the top EdU-positive cells along the crypt-villus axis. The
1196 white bracket shows the distance from the bottom of the crypt to the top of the EdU-positive
1197 cells. Scale bar: 100 μm. (**i**) Enumeration of EdU positive cells per crypt in the control vs.
1198 IL22Fc-treated animals. Vehicle: n = 117 images from 4 animals, IL22Fc: n = 118 images from
1199 4 animals. Unpaired t-test. (**j**) Measurement of the distance from the bottom of the crypt to the
1200 top EdU-positive cells. The migration velocities are coupled to cell proliferation rates[80]. Vehicle:
1201 n = 120 images from 4 animals, IL22Fc: n = 120 images from 4 animals. Unpaired t-test.

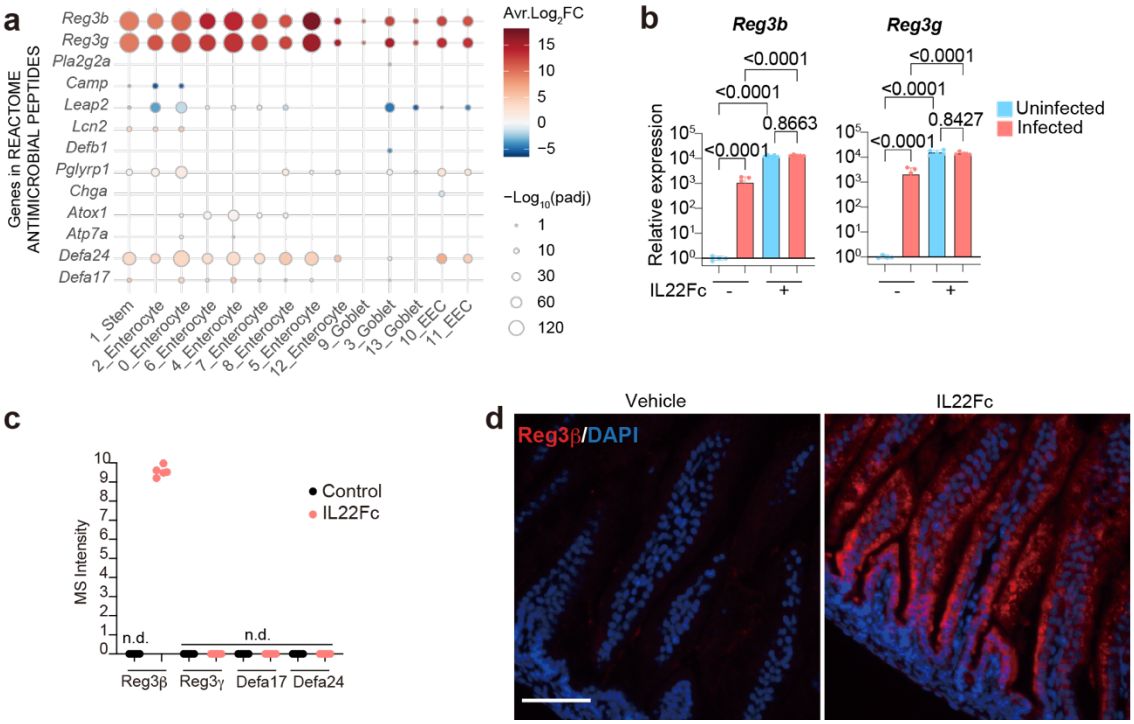

Extended Data Fig. 8. IL22Fc administration increased the expression of Reg3β in the epithelial cells

(a) Relative expression of the DEGs in the Reactome antimicrobial peptide pathway. Color code and the scale of the dot size indicate average $\log_2$ fold change and negative $\log_{10}$ scaled adjusted p-value in IL22Fc-treated animals, respectively. (**b**) qPCR analysis of *Reg3b* and *Reg3g* in the distal SI tissue. Data is normalized by the expression of β-Actin and presented as relative to IL22Fc-untreated/uninfected control. n = 4-5/group. mean ± SD. (**c**) Mass-spectrometry signal intensity of Reg3β, Reg3γ, Defa17 and Defa24 peptides in intestinal wash proteomics analysis in control- (black) vs IL22Fc-treated animals (red). n.d.: not detected. (**d**) Representative images of immunohistochemistry of Reg3β protein (red) and DAPI (blue) in the small intestine from control or IL22Fc-treated animal. Scale bar: 50 μm.

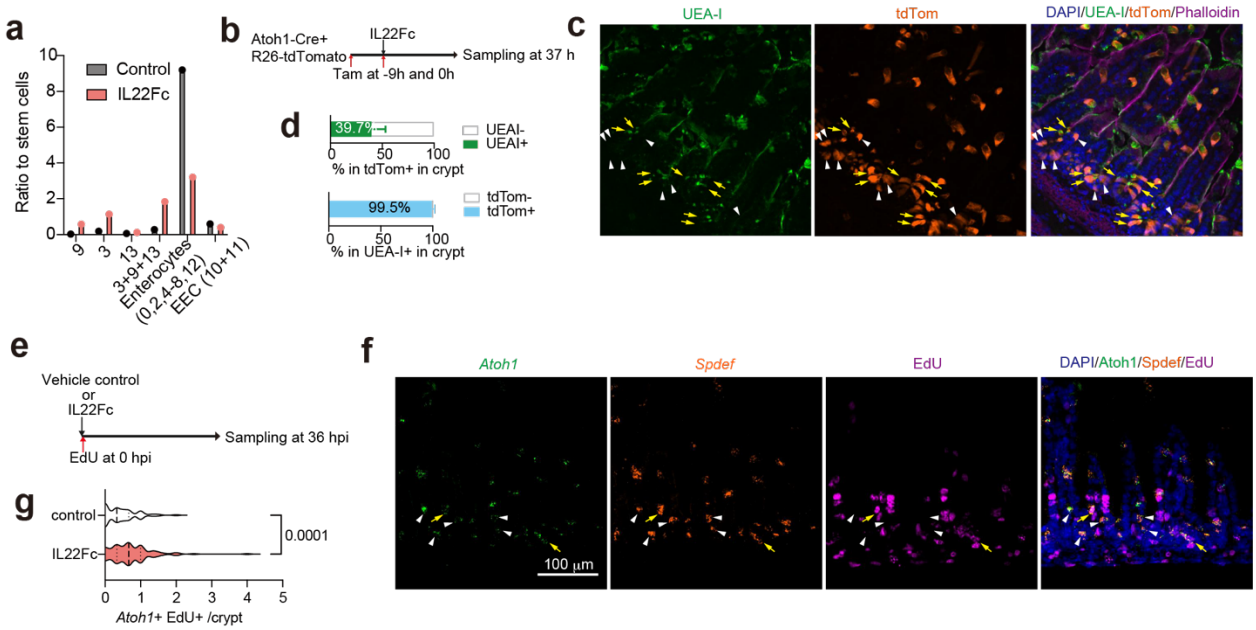

Extended Data Fig. 9 IL22Fc promotes secretory progenitor cells proliferation
(**a**) Ratio between indicated cell cluster vs stem cell clusters in scRNA-seq data in Figure 5a. Cell counts per cluster was divided by the count of stem cells. (**b**) Experimental protocol for testing if IL22Fc-induced crypt associated goblet cell arise from the Atoh1+ secretory lineage in Atoh1Cre(ER-T2);Rosa26RLSL-TdTomato animals. Tamoxifen was administered -9 and 0 post IL22Fc administration. Tissue was sampled 37 h post IL22Fc administration. (**c**) Tissue sections were stained with UEA-I as a marker for mucus+ cells (green), and DAPI (blue). White arrowheads and yellow arrows indicate tdTomato+ UEA-I- cells and tdTomato+ UEA-I+ cells, respectively. (**d**) The percentage of UEA-I+ cells in tdTomato+ cells (top), and tdTomato+ cells in UEA-I+ cells (bottom). (**e**) Experimental protocol for testing if IL22Fc treatment promotes proliferation of crypt-associated *Atoh1*+ cells; EdU was administered at 0 hpi. (f) Tissue was stained with RNA FISH probes for the secretory lineage markers *Atoh1* and *Spdef* and EdU was detected with click chemistry. White arrowheads and yellow arrows indicate *Atoh1*+ EdU- cells and *Atoh1*+ EdU+ cells, respectively. (**g**) Enumeration of *Atoh1*+ EdU+ cells per crypt. 140 and 100 images of the small intestine in control (n = 4) vs IL22Fc-treated animals (n = 4) were analyzed. Welch's t-test. p-value is shown. p-value is shown.

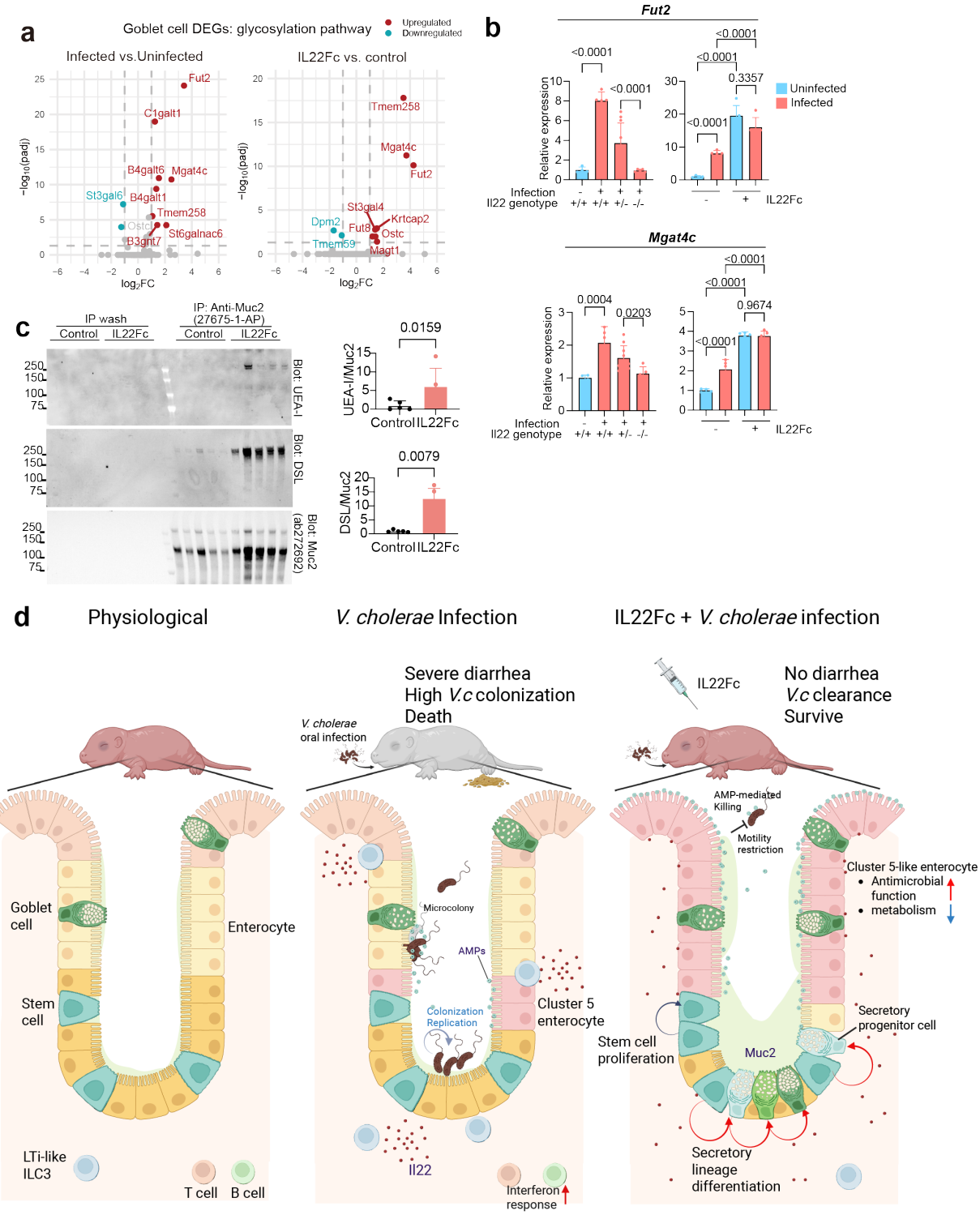

Extended Data Fig. 10. IL22Fc administration modifies mucus and protects against experimental cholerae

(**a**) Volcano plots represent differentially expressed genes associated with glycosylation (GO:0006486) in goblet cells in uninfected vs *V. cholerae* infected (left), or control vs IL22Fc-treated animals in the scRNA-seq data (right). (**b**) Expression of glycosylation genes in the distal

1238 SI tissues in uninfected (n = 4) or *V. cholerae*-infected WT C57BL/6 (+/+) (n = 5), IL22
1239 heterozygous (+/-) (n = 10), or IL22 knockout (-/-) (n = 5) animals (left), and control vs IL22Fc-
1240 treated animals (n = 4-5/group) (right). mean ± SD. One-way ANOVA. (**c**) Western blot image
1241 of immunoprecipitation of Muc2 and its modification with fucose (UEA-I) and *N*-
1242 acetylglucosamine (DSL) in the SI luminal wash. Relative abundance of modification (UEA-
1243 I/Muc2, DSL/Muc2) in Muc2 (250kDa band) is quantified using densitometry and shown as
1244 relative to control (right graph). (**d**) The intestinal response to *V. cholerae* infection and the
1245 mechanism of IL22Fc-mediated protection. Infant mice lack Paneth cells but almost all major
1246 immune cell types are present except for plasma cells (left). *V. cholerae* infection recruits LTi-
1247 like ILC3 to the lamina propria and epithelial layer, and activates IL22 secretion. *V. cholerae*
1248 infection elevates the abundance of a subset of epithelial cells (cluster 5) specialized in defense
1249 responses such as production of Reg3β, which binds *V. cholerae* microcolonies and kills *V.*
1250 *cholerae.* Despite these defense responses, infant mice die from cholera-like diarrhea (middle).
1251 IL22Fc administration induces nearly all enterocyte subsets to express defense associated
1252 phenotypes and antimicrobial function is up-regulated and lipid metabolism is down-regulated.
1253 IL22Fc also promotes differentiation of stem cells into the secretory lineage cell increasing
1254 production of Muc2 mucin. Muc2 restricts *V. cholerae* motility and reduces pathogen association
1255 with the epithelium. These mechanisms impair *V. cholerae* colonization, preventing diarrhea and
1256 death. (Created in https://BioRender.com.)

1257 **Supplementary Table 1. Excel file containing marker genes for clustering in epithelial and**
1258 **immune cell scRNA-seq.**
1259
1260 **Supplementary Table 2. An Excel file containing differentially expressed genes in epithelial**
1261 **cells in the proximal SI comparing uninfected vs *V. cholerae* infected animals.**
1262
1263 **Supplementary Table 3. An Excel file containing differentially expressed genes in epithelial**
1264 **cells in the distal SI comparing uninfected vs *V. cholerae* infected animals.**
1265
1266 **Supplementary Table 4. An Excel file containing differentially expressed genes in immune**
1267 **cells in the proximal SI lamina propria comparing uninfected vs *V. cholerae* infected**
1268 **animals.**
1269
1270 **Supplementary Table 5. An Excel file containing differentially expressed genes in immune**
1271 **cells in the distal SI lamina propria comparing uninfected vs *V. cholerae* infected animals.**
1272
1273 **Supplementary Table 6. An Excel file containing the in vivo Tn-seq analysis result.**
1274
1275 **Supplementary Table 7. An Excel file containing differentially expressed genes in epithelial**
1276 **cells in the distal SI lamina propria comparing IL22Fc-treated vs vehicle-treated animals.**
1277
1278 **Supplementary Table 8. An Excel file containing oligonucleotide sequences for the**
1279 **construction of deletion mutant strains of *V. cholerae* and primer sequences for qPCR**

1280 **References**
1281

1282 1. WHO. External Situation Report n. 22. *Multi-country outbreak of cholera* (2025).

1283 2. Kanungo, S., Azman, A. S., Ramamurthy, T., Deen, J. & Dutta, S. Cholera. *The Lancet*
1284 (2022).

1285 3. Taylor, R. K., Miller, V. L., Furlong, D. B. & Mekalanos, J. J. Use of phoA gene fusions to
1286 identify a pilus colonization factor coordinately regulated with cholera toxin. *Proc. Natl. Acad.*
1287 *Sci.* **84**, 2833–2837 (1987).

1288 4. Ryan, E. T. *et al.* Systemic, Mucosal, and Memory Immune Responses following Cholera.
1289 *Tropical Medicine Infect Dis* **6**, 192 (2021).

1290 5. Levine, M. M. *et al.* Duration of Infection-Derived Immunity to Cholera. *J. Infect. Dis.* **143**,
1291 818–820 (1981).

1292 6. Flach, C.-F. *et al.* Broad Up-Regulation of Innate Defense Factors during Acute Cholera.
1293 *Infect. Immun.* **75**, 2343–2350 (2007).

1294 7. Weil, A. A. *et al.* Posttranslational Regulation of IL-23 Production Distinguishes the Innate
1295 Immune Responses to Live Toxigenic versus Heat-Inactivated Vibrio cholerae. *mSphere* **4**,
1296 e00206-19 (2019).

1297 8. Bourque, D. L. *et al.* Analysis of the Human Mucosal Response to Cholera Reveals Sustained
1298 Activation of Innate Immune Signaling Pathways. *Infect. Immun.* **86**, 10.1128/iai.00594-17
1299 (2018).

1300 9. Qadri, F. *et al.* Acute dehydrating disease caused by Vibrio cholerae serogroups O1 and O139
1301 induce increases in innate cells and inflammatory mediators at the mucosal surface of the gut.
1302 *Gut* **53**, 62 (2004).

1303 10. Qadri, F. *et al.* Increased Levels of Inflammatory Mediators in Children and Adults Infected
1304 with Vibrio cholerae O1 and O139. *Clin. Vaccine Immunol.* **9**, 221–229 (2002).

1305 11. Ellis, C. N. *et al.* Comparative Proteomic Analysis Reveals Activation of Mucosal Innate
1306 Immune Signaling Pathways during Cholera. *Infect. Immun.* **83**, 1089–1103 (2015).

1307 12. Kayama, H., Okumura, R. & Takeda, K. Interaction Between the Microbiota, Epithelia, and
1308 Immune Cells in the Intestine. *The Annual Review of Immunology* (2020) doi:10.1146/annurev-
1309 immunol-070119-115104.

1310 13. Herrington, D. A. *et al.* Toxin, toxin-coregulated pili, and the toxR regulon are essential for
1311 Vibrio cholerae pathogenesis in humans. *J. Exp. Med.* **168**, 1487–1492 (1988).

1312 14. Lueschow, S. R. & McElroy, S. J. The Paneth Cell: The Curator and Defender of the
1313 Immature Small Intestine. *Front Immunol* **11**, 587 (2020).

1314 15. Millet, Y. A. *et al.* Insights into Vibrio cholerae Intestinal Colonization from Monitoring
1315 Fluorescently Labeled Bacteria. *PLoS Pathog.* **10**, e1004405 (2014).

1316 16. Luyendyk, J. P., Schoenecker, J. G. & Flick, M. J. The multifaceted role of fibrinogen in
1317 tissue injury and inflammation. *Blood* **133**, 511–520 (2019).

1318 17. Rogers, A. P., Mileto, S. J. & Lyras, D. Impact of enteric bacterial infections at and beyond
1319 the epithelial barrier. *Nat. Rev. Microbiol.* **21**, 260–274 (2023).

1320 18. Xu, H. *et al.* Transcriptional Atlas of Intestinal Immune Cells Reveals that Neuropeptide α-
1321 CGRP Modulates Group 2 Innate Lymphoid Cell Responses. *Immunity* **51**, 696-708.e9 (2019).

1322 19. Jones, L. O. *et al.* Single-cell resolution of the adult zebrafish intestine under conventional
1323 conditions and in response to an acute Vibrio cholerae infection. *Cell Rep.* **42**, 113407 (2023).

1324 20. Jin, S. *et al.* Inference and analysis of cell-cell communication using CellChat. *Nat Commun*
1325 **12**, 1088 (2021).

1326 21. Aujla, S. J. *et al.* IL-22 mediates mucosal host defense against Gram-negative bacterial
1327 pneumonia. *Nat. Med.* **14**, 275–281 (2008).

1328 22. Zheng, Y. *et al.* Interleukin-22 mediates early host defense against attaching and effacing
1329 bacterial pathogens. *Nat. Med.* **14**, 282–289 (2008).

1330 23. Hasegawa, M. *et al.* Interleukin-22 Regulates the Complement System to Promote Resistance
1331 against Pathobionts after Pathogen-Induced Intestinal Damage. *Immunity* **41**, 620–632 (2014).

1332 24. Nagao-Kitamoto, H. *et al.* Interleukin-22-mediated host glycosylation prevents Clostridioides
1333 difficile infection by modulating the metabolic activity of the gut microbiota. *Nat. Med.* **26**, 608–
1334 617 (2020).

1335 25. Horn, V. & Sonnenberg, G. F. Group 3 innate lymphoid cells in intestinal health and disease.
1336 *Nat. Rev. Gastroenterol. Hepatol.* **21**, 428–443 (2024).

1337 26. Behnsen, J. *et al.* The Cytokine IL-22 Promotes Pathogen Colonization by Suppressing
1338 Related Commensal Bacteria. *Immunity* **40**, 262–273 (2014).

1339 27. Layunta, E., Jäverfelt, S., Dolan, B., Arike, L. & Pelaseyed, T. IL-22 promotes the formation
1340 of a MUC17 glycocalyx barrier in the postnatal small intestine during weaning. *Cell Rep.* **34**,
1341 108757 (2021).

1342 28. Stefanich, E. G. *et al.* Pre-clinical and translational pharmacology of a human interleukin-22
1343 IgG fusion protein for potential treatment of infectious or inflammatory diseases. *Biochem.*
1344 *Pharmacol.* **152**, 224–235 (2018).

1345 29. Hullahalli, K., Pritchard, J. R. & Waldor, M. K. Refined Quantification of Infection
1346 Bottlenecks and Pathogen Dissemination with STAMPR. *mSystems* **6**, e00887-21 (2021).

1347 30. Gardel, C. L. & Mekalanos, J. J. Alterations in Vibrio cholerae motility phenotypes correlate
1348 with changes in virulence factor expression. *Infect. Immun.* **64**, 2246–2255 (1996).

1349 31. Wang, X. *et al.* Interleukin-22 alleviates metabolic disorders and restores mucosal immunity
1350 in diabetes. *Nature* **514**, 237–241 (2014).

1351 32. Lindemans, C. A. *et al.* Interleukin-22 promotes intestinal-stem-cell-mediated epithelial
1352 regeneration. *Nature* **528**, 560–564 (2015).

1353 33. Miki, T., Holst, O. & Hardt, W.-D. The Bactericidal Activity of the C-type Lectin RegIIIβ
1354 against Gram-negative Bacteria involves Binding to Lipid A*. *J. Biol. Chem.* **287**, 34844–34855
1355 (2012).

1356 34. Stelter, C. *et al.* Salmonella-Induced Mucosal Lectin RegIIIβ Kills Competing Gut
1357 Microbiota. *PLoS ONE* **6**, e20749 (2011).

1358 35. Gaudino, S. J. *et al.* IL-22 receptor signaling in Paneth cells is critical for their maturation,
1359 microbiota colonization, Th17-related immune responses, and anti-Salmonella immunity.
1360 *Mucosal Immunol.* **14**, 389–401 (2021).

1361 36. He, G.-W. *et al.* Optimized human intestinal organoid model reveals interleukin-22-
1362 dependency of paneth cell formation. *Cell Stem Cell* **29**, 1333-1345.e6 (2022).

1363 37. Yang, Q., Bermingham, N. A., Finegold, M. J. & Zoghbi, H. Y. Requirement of Math1 for
1364 Secretory Cell Lineage Commitment in the Mouse Intestine. *Science* **294**, 2155–2158 (2001).

1365 38. Peeters, T. & Vantrappen, G. The Paneth cell: a source of intestinal lysozyme. *Gut* **16**, 553
1366 (1975).

1367 39. Kolev, H. M. & Kaestner, K. H. Mammalian Intestinal Development and Differentiation—
1368 The State of the Art. *Cell. Mol. Gastroenterol. Hepatol.* **16**, 809–821 (2023).

1369 40. Johansson, M. E. V. & Hansson, G. C. Immunological aspects of intestinal mucus and
1370 mucins. *Nat. Rev. Immunol.* **16**, 639–649 (2016).

1371 41. Rodriguez, N. R. M. *et al.* Expansion of Paneth Cell Population in Response to Enteric
1372 Salmonella enterica Serovar Typhimurium Infection. *Infect. Immun.* **80**, 266–275 (2011).

1373 42. Campbell, I. W. *et al.* Vibrio cholerae motility is associated with inter-animal transmission.
1374 *Nat. Commun.* **16**, 7989 (2025).

1375 43. Goto, Y. *et al.* Innate lymphoid cells regulate intestinal epithelial cell glycosylation. *Science*
1376 **345**, 1254009 (2014).

1377 44. Melchior, K. *et al.* IL-22-dependent responses and their role during Citrobacter rodentium
1378 infection. *Infect. Immun.* **92**, e00099-24 (2024).

1379 45. Zhu, Q. *et al.* Epithelial dysfunction is prevented by IL-22 treatment in a Citrobacter
1380 rodentium-induced colitis model that shares similarities with inflammatory bowel disease.
1381 *Mucosal Immunol.* **15**, 1338–1349 (2022).

1382 46. Pham, T. A. N. *et al.* Epithelial IL-22RA1-Mediated Fucosylation Promotes Intestinal
1383 Colonization Resistance to an Opportunistic Pathogen. *Cell Host Microbe* **16**, 504–516 (2014).

1384 47. Bergstrom, K. S. B. *et al.* Muc2 Protects against Lethal Infectious Colitis by Disassociating
1385 Pathogenic and Commensal Bacteria from the Colonic Mucosa. *PLoS Pathog.* **6**, e1000902
1386 (2010).

1387 48. Wang, B. X. *et al.* Host-derived O-glycans inhibit toxigenic conversion by a virulence-
1388 encoding phage in Vibrio cholerae. *Embo J* **42**, e111562 (2023).

1389 49. Dupont, A., Heinbockel, L., Brandenburg, K. & Hornef, M. W. Antimicrobial peptides and
1390 the enteric mucus layer act in concert to protect the intestinal mucosa. *Gut Microbes* **5**, 761–765
1391 (2014).

1392 50. Rouard, C. *et al.* Long-Distance Spread of a Highly Drug-Resistant Epidemic Cholera Strain.
1393 *N. Engl. J. Med.* **391**, 2271–2273 (2024).

1394 51. Richterman, A., Sainvilien, D. R., Eberly, L. & Ivers, L. C. Individual and Household Risk
1395 Factors for Symptomatic Cholera Infection: A Systematic Review and Meta-analysis. *J. Infect.*
1396 *Dis.* **218**, S154–S164 (2018).

1397 52. Heida, F. H. *et al.* Paneth cells in the developing gut: when do they arise and when are they
1398 immune competent? *Pediatr. Res.* **80**, 306–310 (2016).

1399 53. Cui, C., Wang, F., Zheng, Y., Wei, H. & Peng, J. From birth to death: The hardworking life
1400 of Paneth cell in the small intestine. *Front. Immunol.* **14**, 1122258 (2023).

1401 54. Wagner, F. *et al.* Dose escalation randomised study of efmarodocokin alfa in healthy
1402 volunteers and patients with ulcerative colitis. *Gut* **72**, 1451–1461 (2023).

1403 55. Waters, M. *et al.* Astegolimab or Efmarodocokin Alfa in Patients With Severe COVID-19
1404 Pneumonia: A Randomized, Phase 2 Trial*. *Crit. Care Med.* **51**, 103–116 (2023).

1405 56. Shi, Z., Ohno, H. & Satoh-Takayama, N. Dietary Derived Micronutrients Modulate Immune
1406 Responses Through Innate Lymphoid Cells. *Front. Immunol.* **12**, 670632 (2021).

1407 57. Fujiyama, T. *et al.* Inhibitory and excitatory subtypes of cochlear nucleus neurons are defined
1408 by distinct bHLH transcription factors, Ptf1a and Atoh1. *Development* **136**, 2049–2058 (2009).

1409 58. Velcich, A. *et al.* Colorectal Cancer in Mice Genetically Deficient in the Mucin Muc2.
1410 *Science* **295**, 1726–1729 (2002).

1411 59. Chen-Shan, C. *et al.* The Origin of the Haitian Cholera Outbreak Strain. *New Engl J Med*
1412 **364**, 33–42 (2011).

1413 60. Chao, M. C. *et al.* A Cytosine Methytransferase Modulates the Cell Envelope Stress
1414 Response in the Cholera Pathogen. *PLoS Genet.* **11**, e1005666 (2015).

1415 61. Fakoya, B. *et al.* Nontoxigenic Vibrio cholerae Challenge Strains for Evaluating Vaccine
1416 Efficacy and Inferring Mechanisms of Protection. *mBio* **13**, e00539-22 (2022).

1417 62. Leitner, D. R., Zingl, F. G., Morano, A. A., Zhang, H. & Waldor, M. K. The Mla pathway
1418 promotes Vibrio cholerae re-expansion from stationary phase. *mBio* **16**, e03433-24 (2024).

1419 63. Manno, G. L. *et al.* RNA velocity of single cells. *Nature* **560**, 494–498 (2018).

1420 64. Bergen, V., Lange, M., Peidli, S., Wolf, F. A. & Theis, F. J. Generalizing RNA velocity to
1421 transient cell states through dynamical modeling. *Nat. Biotechnol.* **38**, 1408–1414 (2020).

1422 65. Hubbard, T. P. *et al.* A live vaccine rapidly protects against cholera in an infant rabbit model.
1423 *Sci Transl Med* **10**, (2018).

1424 66. Chao, M. C., Abel, S., Davis, B. M. & Waldor, M. K. The design and analysis of transposon
1425 insertion sequencing experiments. *Nat. Rev. Microbiol.* **14**, 119–128 (2016).

1426 67. Hullahalli, K. & Waldor, M. K. Pathogen clonal expansion underlies multiorgan
1427 dissemination and organ-specific outcomes during murine systemic infection. *eLife* **10**, e70910
1428 (2021).

1429 68. Liang, Z. *et al.* Protocol to profile spatially resolved NLRP3 inflammasome complexes using
1430 APEX2-based proximity labeling. *STAR Protoc.* **5**, 103417 (2024).

1431 69. Peng, J. & Gygi, S. P. Proteomics: the move to mixtures. *J. Mass Spectrom.* **36**, 1083–1091
1432 (2001).

1433 70. Eng, J. K., McCormack, A. L. & Yates, J. R. An approach to correlate tandem mass spectral
1434 data of peptides with amino acid sequences in a protein database. *J. Am. Soc. Mass Spectrom.* **5**,
1435 976–989 (1994).

1436 71. Tyanova, S., Temu, T. & Cox, J. The MaxQuant computational platform for mass
1437 spectrometry-based shotgun proteomics. *Nat. Protoc.* **11**, 2301–2319 (2016).

1438 72. Tyanova, S. *et al.* The Perseus computational platform for comprehensive analysis of
1439 (prote)omics data. *Nat. Methods* **13**, 731–740 (2016).

1440 73. Haber, A. L. *et al.* A single-cell survey of the small intestinal epithelium. *Nature* **551**, 333–
1441 339 (2017).

1442 74. Andreatta, M. & Carmona, S. J. UCell: Robust and scalable single-cell gene signature
1443 scoring. *Comput. Struct. Biotechnol. J.* **19**, 3796–3798 (2021).

1444 75. Schaum, N. *et al.* Single-cell transcriptomics of 20 mouse organs creates a Tabula Muris.
1445 *Nature* **562**, 367–372 (2018).

1446 76. Franzén, O., Gan, L.-M. & Björkegren, J. L. M. PanglaoDB: a web server for exploration of
1447 mouse and human single-cell RNA sequencing data. *Database* **2019**, baz046 (2019).

1448 77. Koprivica, I. *et al.* ILC3: a case of conflicted identity. *Front. Immunol.* **14**, 1271699 (2023).

1449 78. Scott, C. L., Bain, C. C. & Mowat, A. M. Inflammation, Methods and Protocols. *Methods*
1450 *Mol. Biol.* **1559**, 223–239 (2017).

1451 79. Vivier, E. *et al.* Innate Lymphoid Cells: 10 Years On. *Cell* **174**, 1054–1066 (2018).

1452 80. Parker, A. *et al.* Cell proliferation within small intestinal crypts is the principal driving force
1453 for cell migration on villi. *FASEB J.* **31**, 636–649 (2017).

1454